CONTRIBUTED REPORT CR-10-D

Arizona Geological Survey
www.azgs.az.gov

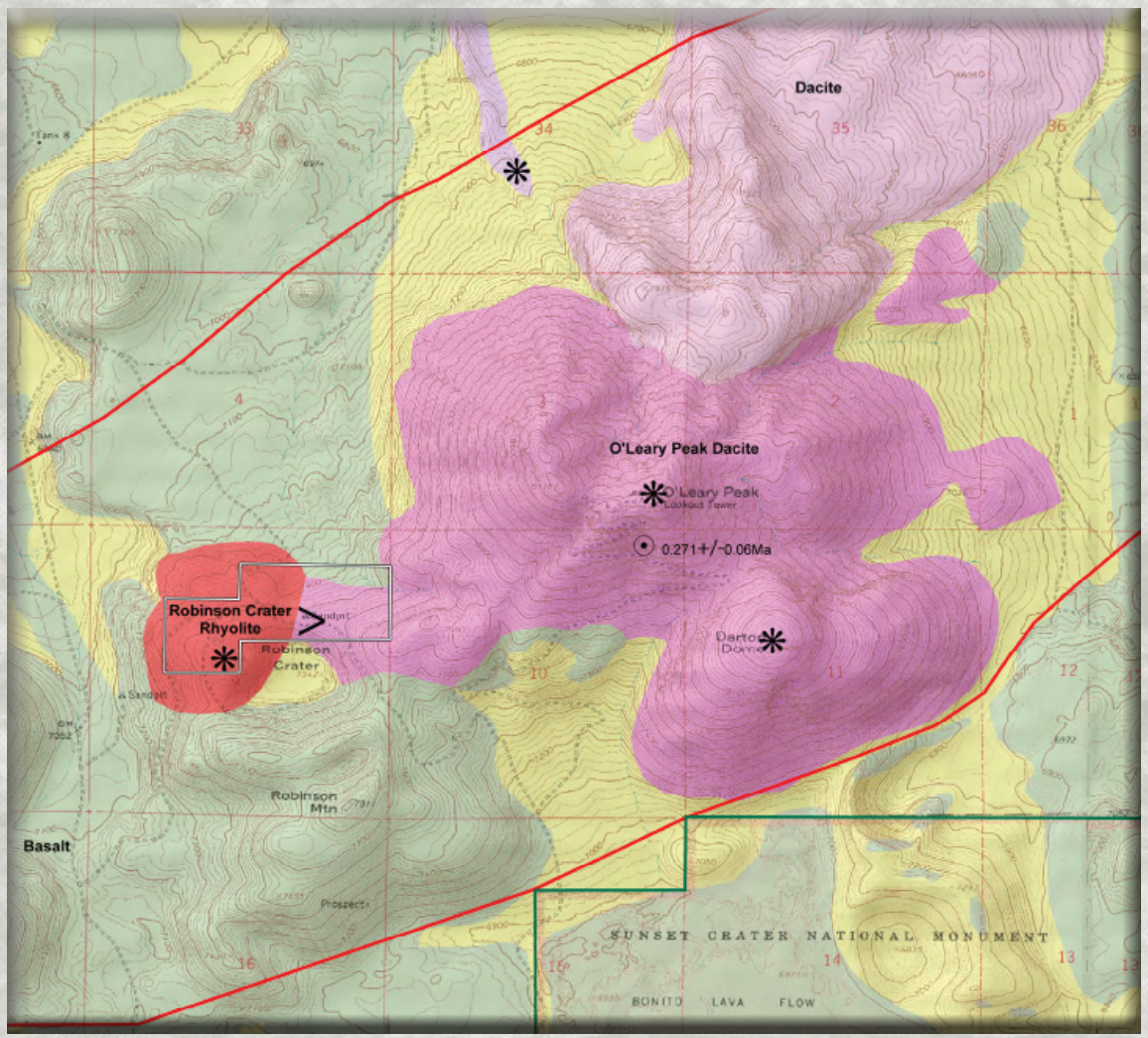

GEOTHERMAL RESOURCES EVALUATION PROGRAM OF THE EASTERN SAN FRANCISCO VOLCANIC FIELD, ARIZONA

Paul Morgan, John H. Sass and Wendell Duffield
Dept. of Geology, Northern Arizona University

February 2010

Geothermal Resource Evaluation Program of the Eastern San Francisco Volcanic Field, Arizona

Paul Morgan, John H. Sass and Wendell Duffield
Dept. of Geology, Northern Arizona University

with contributions from
[1]Tracey Felger, [1]Bill Fry and [2]Lisa Peters
[1]Northern Arizona University
[2]New Mexico Geochronological Research Laboratory

2010

Arizona Geological Survey Contributed Report Series

Final Report to the Department of Energy, Project GRED II

Phase I

Geothermal Resource Evaluation Program of the Eastern San Francisco Volcanic Field, Arizona

Agreement # DE-FC04-2002AL68298

by

Paul Morgan, John H. Sass, and Wendell Duffield

Department of Geology, Northern Arizona University

with contributions from

Tracey Felger and Bill N. Fry

Department of Geology, Northern Arizona University

and age data report by

Lisa Peters

New Mexico Geochronological Research Laboratory

May, 2004

P.I.: Paul Morgan

Department of Geology
Box, 4099, Frier Hall, Bldg. 12, Knoles Drive
Northern Arizona University, AZ 86011-4099
Tel: (928) 523-7175. Fax: (928) 523-9220
Paul.Morgan@nau.edu

Geothermal Resource Evaluation Program of the Eastern San Francisco Volcanic Field, Arizona

Executive Summary

The *Geothermal Resource Evaluation Program of the Eastern San Francisco Volcanic Field, Arizona*, has been a fifteen-month study collecting and evaluating geological and geophysical data to assess the potential for a geothermal resource in this region. The San Francisco Volcanic Field has been recognized as a target for geothermal exploration for more than thirty years, primarily based on the volume and youth of volcanic rocks in the field. Interest has never progressed to the stage of drilling, however, because the field lacks surface geothermal manifestations, such as geysers, hot springs, or fumaroles. Cold water springs are also absent in the field because it is a recharge area for the regional aquifer system, and a working hypothesis at the beginning of this project was that a deep thermal system was masked beneath the shallow recharge system. Previous studies have provided strong evidence that there is heat, and perhaps partial melt from the eruption of the San Francisco Peaks in the deep crust.

Geothermal systems that are currently economically exploited for electricity generation have elevated geothermal gradients in the upper crust and either young shallow silicic intrusions and/or deep groundwater circulation systems. In this study we have therefore focused our investigations in the eastern portion of the volcanic field where the volcanism is youngest, and in particular along an east-northeast line of the three youngest silicic volcanic features immediately north of Sunset Crater, Sugarloaf Mountain, O'Leary Peak, and Strawberry Crater. We have collected new age dates from the rocks of these features to confirm their youthful ages, we have improved existing geologic mapping, compiled new groundwater chemistry data, and improved the coverage of existing gravity data to supplement other data sets to analyze this area. We have also been able to supplement the results of our study with an independent study of groundwaters and travertine deposits from these groundwaters in the Grand Canyon that are partially derived from beneath the San Francisco Volcanic Field. The new comprehensive analysis of this study strongly supports the two-layer hydrologic model in which a deeper geothermal system is masked by a shallow groundwater recharge system. Unfortunately, none of the data in this analysis gives direct size or temperature information concerning the deep geothermal system.

Crude estimates of temperatures within the deep geothermal system suggest that temperatures should be sufficient for economic electricity generation using a binary system. Using a conservative conceptual conductive cooling model of a silicic intrusion, we have estimated temperatures of 125-150°C (255-300°F) at about 3 km (10,000 feet). These estimates are based on many assumptions, poorly constrained by data, however. The only way that temperatures and permeability of the resource can be determined is by drilling. We believe that the data compiled in this study present a strong case for continuing this project into the next phase, which would be to drill a slim hole to a depth of ~2.5-3.0 km (~8,000-10,000 feet) to test temperatures and permeabilities in the deep geothermal system. A drilling site exists within the target area that is on a privately owned patented mining claim, and the next phase of the project can proceed as soon as funding is available

Table of Contents

continued …

Note:
Tables and Figures from the appendices are not included in the lists of Tables and Figures below.

List of Tables

Page

List of Plates and Figures

Page

Plates

Figures

continued …

Geothermal Resource Evaluation Program of the Eastern San Francisco Volcanic Field, Arizona

Introduction

The San Francisco Volcanic Field (SFVF) in northern Arizona has attracted attention as a potential electricity-grade geothermal resource since at least the mid-1970s when parts of it were designated at a Known Geothermal Resource Area (KGRA) on the basis of competitive bidding activity for geothermal leases in the field. In general, the strong indicators for a geothermal resource are the young volcanism, less than 1000-years old, the youngest in Arizona, and the size of the field.

However, there are no surface geothermal manifestations, a rare, perhaps unique absence in a volcanic field so young. Not only are geothermal manifestations absent in the San Francisco geothermal field, cold perennial springs are also absent and the field is basically a recharge area for groundwater with a regionally low water table. A logical solution to the lack of geothermal manifestations is the heat from a deeper geothermal system is masked by a shallow recharge system. This situation presents a very difficult exploration target.

This report compiles, interprets and reinterprets old and new geological, hydrological, geophysical, and geochemical data from the San Francisco Volcanic Field (*Current State of Knowledge*). Specifically the report focuses on the eastern portion of the field, the locus of most recent volcanic activity, with the goal of determining the potential for the presence of a geothermal resource beneath a shallow recharge system. Following a compilation and interpretation of new and existing data a *Conceptual Model* is developed to present an estimate of temperatures in a deep (2-3 km; 7,000-10,000 feet) geothermal system beneath the shallow recharge system. *Recommendations for Further Studies* are then presented, followed by possible parameters for a *Phase II* drilling project to follow the present study.

1. CURRENT STATE OF KNOWLEDGE

GEOLOGY

Introduction

The San Francisco Volcanic Field (SFVF) is located on the Colorado Plateau, near the southwestern margin of this geomorphic province (Figure 1). It is about equidistant (roughly forty-five kilometers) from the Grand Canyon to the north and the Verde Valley to the south. The Verde Valley is the beginning of a north-south transitional zone between the Colorado Plateau and the Basin and Range geomorphic provinces.

The SFVF overlies a kilometer-thick sequence of horizontal Paleozoic and Mesozoic sedimentary rocks, which, in turn, unconformably overlie a granitic/metamorphic

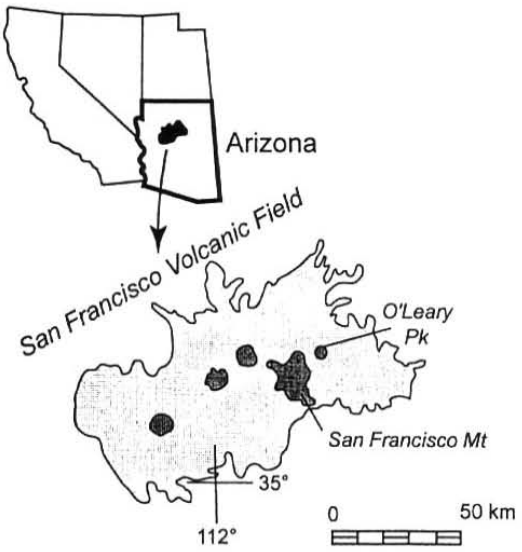

Figure 1. Location of the San Francisco Volcanic Field in northern Arizona

Precambrian basement complex. (Figure 2). The Paleozoic and Precambrian parts of these volcanic underpinnings are well exposed in the walls of the nearby Grand Canyon. Within the SFVF itself, however, outcrops of the pre-volcanic rocks consist of small scattered patches of Mesozoic and uppermost Paleozoic formations.

The SFVF defines an east- to northeast-trending belt that is about one hundred kilometers long and thirty-to-forty kilometers wide. The boundaries of the SFVF are readily visible on a digital elevation model (Figure 3 and Plate 1); the SFVF terrain is expressed as a hilly to mountainous landscape studded with volcanoes of various sizes and shapes, built atop a nearly planar surface on the underlying pre-Cenozoic sedimentary sequence.

The SFVF covers an area of about five thousand square kilometers, and the volume of volcanic rocks is about five hundred cubic kilometers (Ulrich, 1984; Wolfe, 1990). Rock compositions range from basalt to andesite to dacite to rhyolite. Basalt is dominant volumetrically. Wolfe et al. (1987) have mapped the SFVF at a scale of 1:50,000. San Francisco Mountain, the largest volcano of the SFVF, has also been mapped at 1:24,000 (Holm, 1988). More than six hundred volcanoes have been identified (Tanaka et al., 1986). Most are basalt cinder cones with associated small-volume lava flows. Other small volcanoes likely exist, buried by somewhat larger and younger neighbors.

About a dozen intermediate to silicic (andesite, dacite, rhyolite) centers are distributed across the SFVF. These are the largest in volume and tallest volcanoes of the field. At 3,851 m (12,633 feet) above sea level, the summit of San Francisco Mountain stratovolcano is the highest elevation in Arizona (Figure 3 and Plate 1).

The age of volcanism in the SFVF ranges from Pliocene to Holocene (Wolfe, 1990). The oldest volcanoes have yielded K-Ar ages between about 6 Ma and 5 Ma (Wolfe et al., 1987). The youngest eruption occurred about 950 years ago (Smiley, 1958). This eruption created a new basaltic cinder cone (Sunset Crater), fed two small-volume lava flows, and blanketed several hundred square kilometers of the surrounding area with a fallout deposit of cinders. Native Americans were living in the area at the time. An oral

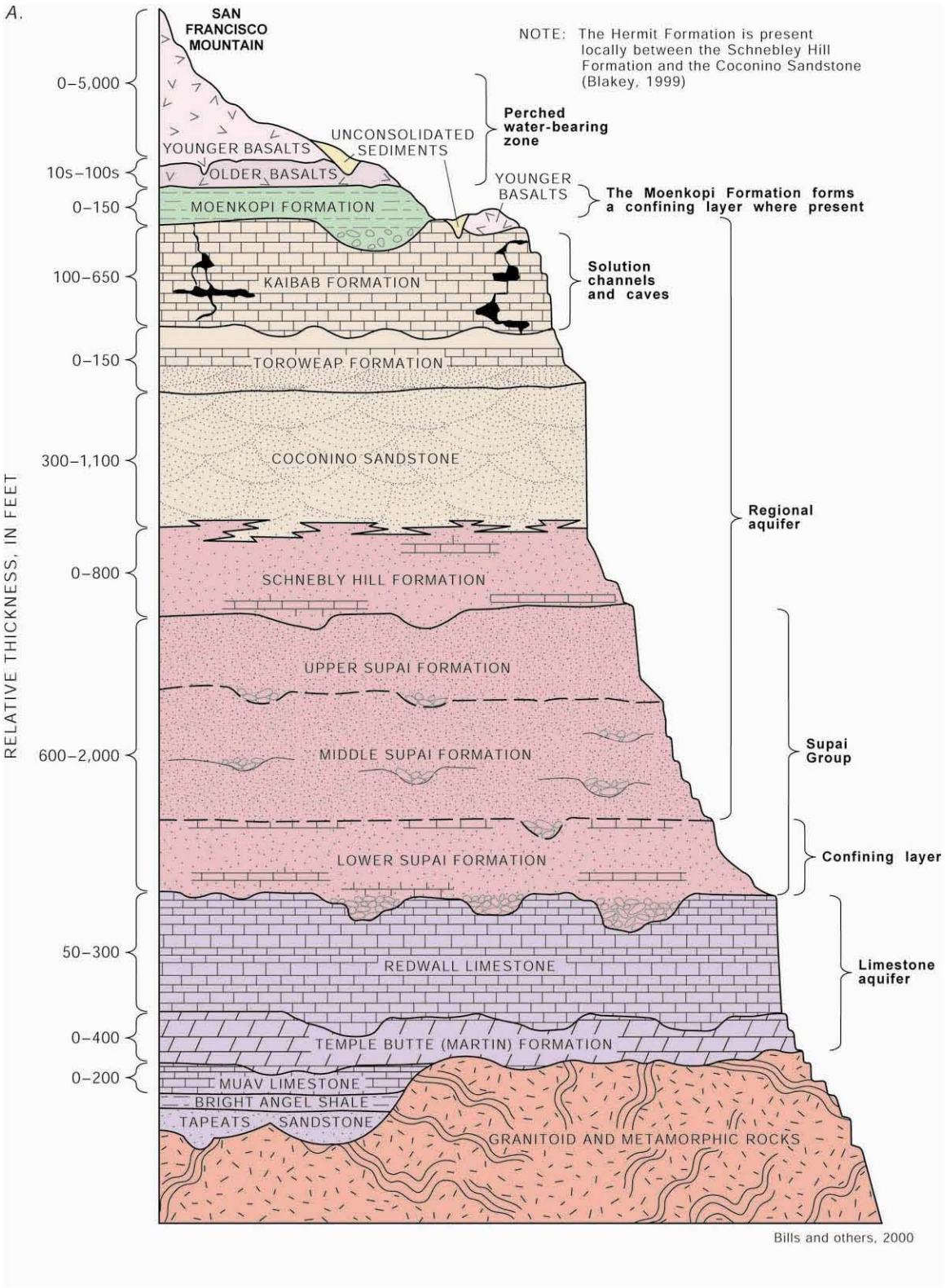

Figure 2. Schematic cross-section of the sedimentary section below the San Francisco Volcanic Field [from Bills et al., 2000].

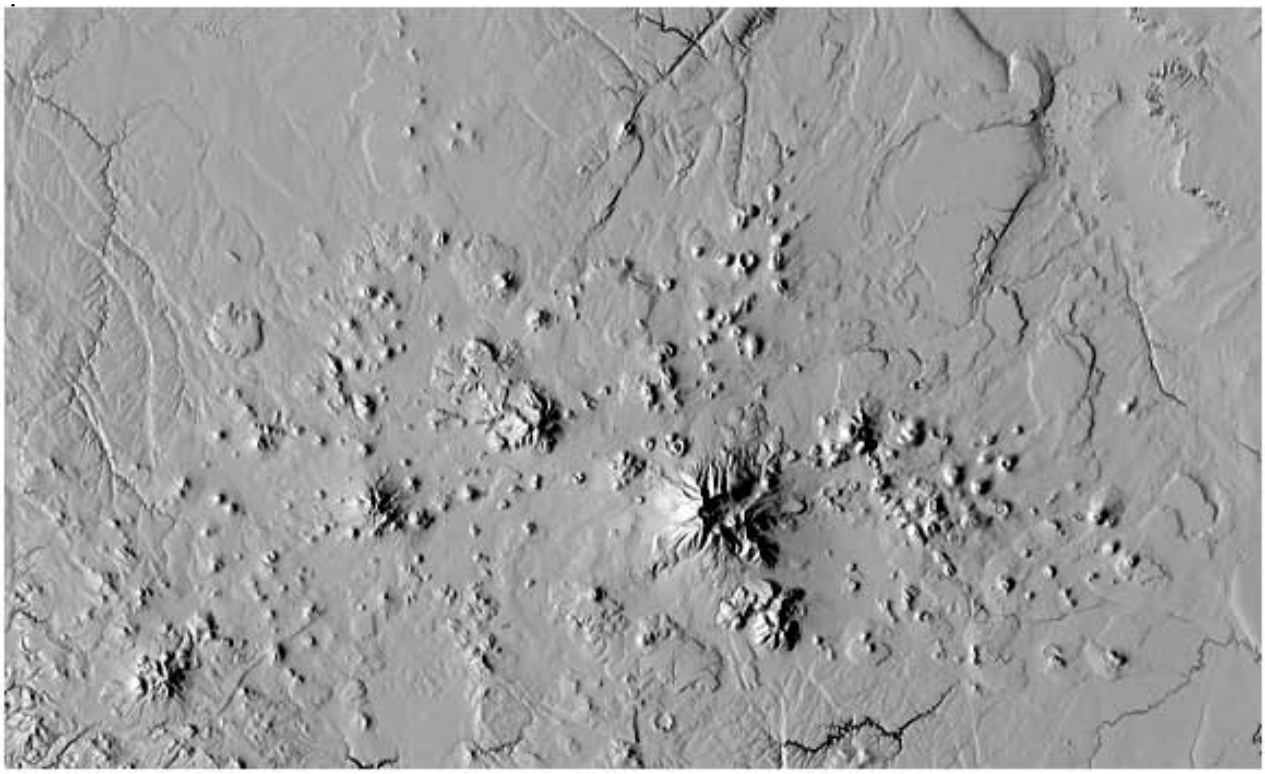

Figure 3. Digital elevation model of the SFVF and adjacent areas. Areas at the southeast, east, and northwest margins of the image are underlain by pre-volcanic horizontal sedimentary rocks that are variably etched by drainage channels, joints, and fault scarps.

tradition that describes the eruption has been passed across many generations to become part of current Hopi culture (Malotki and Lomatuway'ma, 1987).

Based on dendrochronology, Smiley (1958) reported that the eruption that created Sunset Crater began during the winter of 1064-1065 AD. Ongoing reinvestigation of this age, based principally on paleomagnetic secular variation recorded by erupted products, suggests that eruption occurred between 1040 AD and 1100 AD (Ort et al., 2002), consistent with the tree-ring age reported by Smiley (1958). The duration of the eruption is unknown, but is thought to be a few years at most (Self, 1990; Ort et al., 2002).

Tanaka et al. (1986) have shown that the SFVF developed as a zone of active volcanism which migrated east northeastward at an average rate of between one and three centimeters per year, during the past six million years (Plate 1). This eastward sweep is statistically valid for a broad zone of activity, but includes exceptions when viewed on a volcano-by-volcano basis. For example, Sunset Crater is the youngest volcano in the entire field, but several somewhat older volcanoes lie to the east (Wolfe et al., 1987).

Luedke and Smith (1978) have shown that east northeastward migration of late Cenozoic volcanism is characteristic of volcanic areas scattered over the southwestern sector of the Colorado Plateau. This regional pattern of migration may have developed in response to enlargement of the Basin and Range geomorphic province, as Basin and Range faulting advances incrementally eastward and promotes the formation, rise, and eruption of magmas in the process. The Mesa Butte and Doney faults, which traverse the SFVF (Figure

3 and Plate 1), may be examples of an eastward tectonic advance of Basin and Range structures into the Colorado Plateau.

Project Study Area

Most geothermal resources capable of powering turbine generators are located in areas of Quaternary volcanism. The fundamental reason behind this common association is simple. Magma that cools within the crust transiently heats surrounding water-saturated permeable rock to temperatures sufficient for exploitation to generate electricity.

Nearly all magmas originate in the mantle and are basaltic (Wilson, 1989). Such magmas commonly rise buoyantly from their source region, pass uninterrupted through the crust, and erupt. This scenario applies to the more than six hundred basaltic cinder cones and their lava flows that constitute the bulk of the SFVF. However, when a batch of mantle-derived basaltic magma becomes lodged in the crust, it may evolve to intermediate and silicic compositions by partial melting and assimilation of adjacent wall rocks, by fractional crystallization, or by a combination of these processes (Hildreth, 1981). The most important consequence of such magmatic evolution, for geothermal prospecting, is that the presence of young silicic volcanic rocks at the surface implies an equally young magma reservoir in the underlying crust.

This simple model relating silicic volcanic rocks to a crustal geothermal heat source is a first-order guide in exploring for areas of promising geothermal-energy potential of electrical grade. Other factors being equal, the younger, more voluminous, and aerially concentrated such silicic volcanism is, the greater the chance for discovering a developable geothermal resource in the root zone of the silicic vents. We selected our project study area principally on the basis of this model.

As mentioned earlier, most silicic volcanic rocks of the SFVF are concentrated at a few principal centers. The largest of these, from west to east (older to younger), are Bill Williams Mountain, Sitgreaves Mountain, Kendrick Peak, and San Francisco Mountain (Figure 3). Another area of silicic vents and their erupted products forms an east-northeast pointing finger that extends eastward from San Francisco Mountain (Plates 1 and 2). This nine by four kilometer area of silicic-volcanic-rich real estate is the target of our studies. With the exception of a forty-acre patented claim near the center of this target, all the land is public and part of the Coconino National Forest. The forty-acre patented claim is private land from which rhyolite is currently quarried for hard-rock aggregate. The land owners also hold surface and subsurface mining rights and are very supportive of the current geothermal project.

Chemical Compositions, Ages, and Resource Implications of Volcanic Rocks

Rhyolite and dacite lava domes and flows and their vents cover about forty percent of the target area. Additional young silicic lavas and their vents are located just outside the target area, to the northeast, north, and southwest (Plate 2). Basaltic and andesitic cinder cones and their associated lava flows cover most of the rest of the area. Erosional remnants of fallout cinders from the 950-year-old eruption of nearby Sunset Crater volcano mask some of the bedrock geology. Table 1 presents whole-rock major-element analyses for the range of lava types within and adjacent to the target area.

Smith and Shaw (1979) evaluated many Quaternary volcanic fields in the western USA in support of a national assessment of geothermal resources carried out by the U.S.

Weight % Oxide	Qbb 3808	Qdmd 4826	Qodd 3810D	Qorr 3809B	Qsgr 3723B
SiO_2	49.93	67.16	70.51	72.21	75.64
Al_2O_3	18.99	16.27	15.00	15.49	13.49
Fe_2O_3	1.73	0.96	0.71	0.58	0.27
FeO	8.90	3.30	2.22	1.77	0.75
MgO	4.74	0.60	0.60	0.09	0.06
CaO	8.54	2.49	1.59	0.94	0.57
Na_2O	3.88	5.69	5.20	4.95	4.27
K_2O	0.82	2.79	3.60	3.75	4.93
TiO_2	1.71	0.41	0.34	0.11	0.02
P_2O_5	0.57	0.18	0.14	0.05	0.00
MnO	0.17	0.15	0.09	0.05	0.00

Table 1. Whole-rock analyses of characteristic rock types in and adjacent to the target area. Map units (e.g., Qbb), sample numbers (e.g., 3809B), and analyses are from: Wolfe, E.W., Ulrich, G.E., Holm, R.F., Moore, R.B., and Newhall, C.G., 1987, Geologic Map of the Central Part of the San Francisco Volcanic Field, North Central Arizona: U.S. Geological Survey Map MF-1959, 1:50,000. Moore, R.B., and Wolfe, E.W., 1997, Geologic Map of the East Part of the San Francisco Volcanic Field, North-Central Arizona: U.S. Geological Survey Map MF-1960, 1:50,000. Qbb = Late Pleistocene basalt. Qdmd = Deadman Mesa Dacite. Qodd = O'Leary Peak Dacite. Qorr = Robinson Crater Rhyolite. Qsgr = Sugarloaf Rhyolite.

Geological Survey during the 1970s. As part of their study, they developed a geologic model wherein for every volume of silicic magma that erupts, ten volumes remain in the source magma reservoir lodged in the crust. On the basis of this model, and with knowledge of the numerical age and eruption temperature of the youngest silicic rocks of a given volcanic field, they calculated the present-day temperature and volume (and therefore content of thermal energy) of underlying crustal magma (or pluton, if sufficient time had elapsed for solidification) with reference to a spectrum of conductive and convective cooling scenarios (Smith et al., 1978). They then categorized the volcanic/magmatic systems into three groups (Smith and Shaw, 1979): (1) A group judged to represent active and dormant volcanic systems (considerable geothermal-resource potential), (2) A group that represents extinct volcanic systems (little or no geothermal resource potential), and (3) A group transitional between these two (uncertain geothermal potential). They summarized these groupings on a plot of age of youngest silicic eruption versus volume of underlying crustal magma body at that time for each volcanic field (Smith and Shaw, 1979; Figure 4 this paper).

Their evaluation of the eastern (youngest) silicic part of the SFVF (includes our target area) suggests a geothermal potential similar to volcanic fields at Long Valley and Coso in California, and at the Valles Caldera of New Mexico, all of which have geothermal resources of electrical grade known from drilling. (Figure 4). Thus, in terms of the amount and age of silicic volcanic rocks, our target area is quite favorable with respect to the Smith/Shaw analysis. Also of note is the fact that the SFVF is the only area of Quaternary volcanism in Arizona that includes silicic rocks (Smith and Shaw, 1979; Duffield et al., 2000).

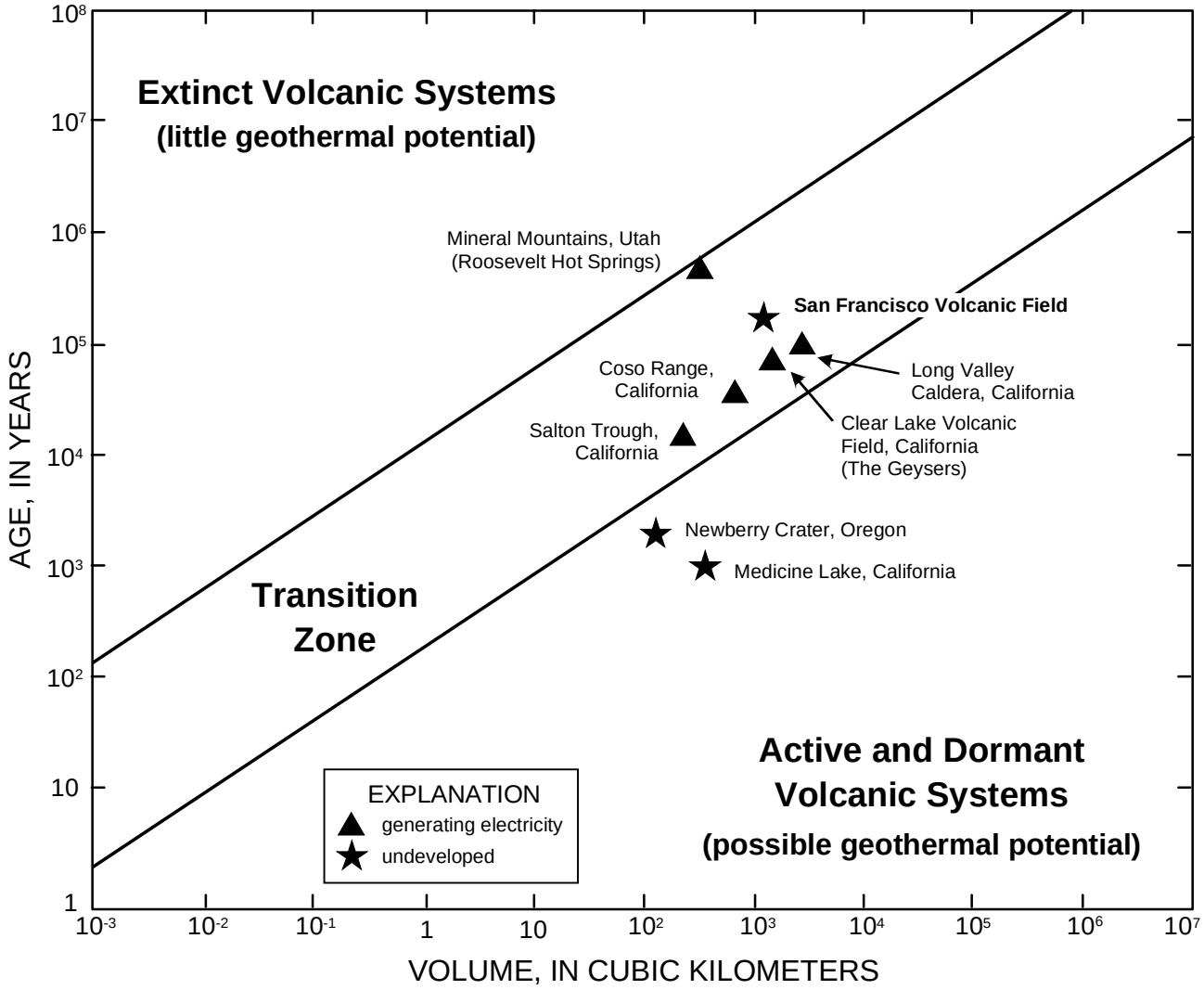

Figure 4. Age of youngest silicic volcanism versus estimated volume of underlying crustal magma at that time, for selected volcanic fields analyzed by Smith and Shaw (1979). Note that the SFVF is surrounded by fields with proven geothermal resources.

When Smith and Shaw carried out their geothermal evaluation of the SFVF, state-of-the-art numerical-age determination for the volcanic rocks was done by the K-Ar technique. At that time, geochronologists recognized that some samples yielded K-Ar ages older than their eruption ages, because these samples contained ^{40}Ar from the mantle source region of magma (so-called excess argon). Some of that excess argon was trapped in glassy groundmass and/or in melt inclusions of phenocrysts of the lavas thus adding pre-existing ^{40}Ar to that produced by the radioactive decay of ^{40}K after eruption (Dalrymple and Hirooka, 1965; Damon et al., 1967).

In view of the possibility that the Smith and Shaw geothermal evaluation of the SFVF included K-Ar ages calculated from samples with excess argon, and thereby unwittingly misrepresented the current thermal status the SFVF crustal magmatic/plutonic body, we have dated four silicic eruptive units in and near our target area by the $^{40}Ar/^{39}Ar$ step-heating technique (Table 2). If a sample is contaminated (be it

Rock Unit	Damon K-Ar Age	40/39 Ar Age	Comparison	Magnetic Polarity
Sugarloaf Rhyolite	0.22 ± 0.02 Ma	0.091 ± 0.002 Ma	40/39 < K-Ar	ND
Strawberry Crater Dacite	0.051 ± 0.046 Ma	0.13 ± 0.04 Ma	Same ±	Normal
Deadman Mesa Dacite	0.17 ± 0.04 Ma	0.25 ± 0.03 Ma	Same ±	ND
O'Leary Peak Dacite	0.25 ± 0.04 Ma	0.271 ± 0.06 Ma	Same ±	ND

Table 2. Potassium-Argon and $^{40}Ar/^{39}Ar$ ages of four silicic volcanic rocks in and adjacent to the study area for this project. For additional analytical data for K-Ar ages see Damon et al., (1974). For additional analytical data for $^{40}Ar/^{39}Ar$ ages see Peters (2003) and Appendix A1 of this report. ND = no determination.

excess argon from the mantle, or older rock assimilated into magma as it traverses the crust), this technique generally yields widely divergent ages for the different temperatures to which the sample is heated. The four silicic units for which we determined age dates were part of the age-data set used by Smith and Shaw.

The results of our $^{40}Ar/^{39}Ar$ age determination suggest minor contamination of the samples (see Appendix 1). Within one-sigma uncertainties for each of the four samples, only one measurable difference appears between the K-Ar ages reported by Smith and Shaw and the new $^{40}Ar/^{39}Ar$ ages (Table 2). Of potential geothermal significance, this one difference is for the youngest (K-Ar) age that Smith and Shaw reported, and therefore was the basis for their geothermal evaluation of the SFVF. Our age (0.091 ± 0.002 Ma, Table 2) for that volcano (Sugarloaf rhyolite dome) is less than half the K-Ar age used by Smith and Shaw.

Within the context of the Smith/Shaw model, a younger age indicates less time for magma of that age to cool, and therefore implies greater present-day potential for a geothermal resource. However, whether a greater potential exists or not also depends on the volume of magma in the crust at the time of the youngest silicic eruption. Smith et al. (1978) remarked that the volume used in their analysis of the SFVF is "highly speculative," with the implication that their value may be too high. If this is so, the volume error would offset their result in a sense opposite to that of an error caused by their youngest eruption age being too old. We have no basis to attempt to modify their volume since the relative magnitudes of potential age and volume offsets are unknown, we also have no basis to modify the original results reported by Smith and Shaw. We simply concur with their finding that a potential for a geothermal resource beneath the youngest silicic part of the SFVF is comparable to potentials associated with volcanic fields of similar age and volume characteristics (Figure 4). We emphasize that several such fields have geothermal resources, proven by drilling subsequent to the study of Smith and Shaw.

Structure

No faults are visible at the surface within the target area, almost certainly because very young volcanic rocks cover the entire area. Nonetheless, the area is strongly imprinted with an east-northeast trending structural fabric defined by vent shape and distribution, and by the pattern of contours on a map of Bouguer gravity (See *Gravity and Magnetic Studies*).

A concentration of silicic domes and lava flows was of first-order importance in defining the target area. From southwest to northeast these are Robinson rhyolite lava dome, O'Leary Peak dacite lava dome, and the vent for Deadman Mesa dacite lava flow (Plate 2). These silicic vents are aligned parallel to the trend of Bouguer gravity anomalies (see *Gravity and Magnetic Studies*). We interpret this alignment to result from control by a system of faults, not visible at the surface because they are buried by the products of magma erupted through them. Eruption of basalt and minor dacite to form Strawberry Crater and its lava flow, just outside the target area to the northeast, marks a continuation of this structurally controlled trend of vents.

San Francisco Mountain, the only stratovolcano and the largest volcano in the SFVF, is on strike with the long axis of our target area, immediately to the west southwest. The footprint of this mountain is elongated parallel to and aligned with the axis of the target area. This shape is likely the result of the relative ease for magma to rise at various locations along east northeast-trending eruptive fissures as the mountain grew. The only faults that Holm (1988) shows on his geologic map of San Francisco Mountain trend east northeast and cut across the central part of the mountain.

What was almost certainly an original east-northeast-elongated conical form of San Francisco Mountain stratovolcano is now highly modified by a mile-wide and three-mile-long amphitheater-shaped feature called the Inner Basin (Figure 3 and Plate 1). This basin opens to the east northeast, directly toward our target area. The basin is thought to have originated during a powerful east-northeast-directed eruption, similar to the eruption that blew away the side of Mount St. Helens stratovolcano in 1980 (Chronic, 2003; Duffield, 1997). Minor stream and glacier erosion have modified the original amphitheater shape.

Subsequent to the formation and minor erosional modification of the Inner basin, a rhyolite lava dome (Sugarloaf of Tables 1, 2) was emplaced at the entrance to the basin, on strike with the faults mapped by Holm (1988). A 122 m (400-foot) late Pleistocene basalt cinder cone is on strike with the lava dome, about 2.4 km (1.5 miles) to the east northeast. Similar to the shape of the footprint of San Francisco Mountain, this cinder cone is elongated in an east northeast direction. Eruptions that formed the elongate cinder deposit at the vent must have been from an east northeast trending fissure to give rise to this shape. This is yet another expression of a strong dominant structural fabric that characterizes the area.

In summary, foot-print shapes of volcanoes, alignment of vents, mapped faults, and the trend of Bouguer gravity anomalies show that our target area is within a zone of east northeast trending faults. Alignment of nearby basalt cinder cones, including Sunset Crater volcano, strongly suggest similar structural control, but by north northwest trending faults (Figure 3, Plate 1). The alignment that includes Sunset Crater projects directly at O'Leary Peak near the center of our target area. Thus, two sets of faults cross the target area. This evidence of faults and fault intersections greatly enhances the possibility for sufficient

permeability for vigorous hydrothermal circulation, if a hydrothermal convection system is present.

HYDROLOGY

The regional hydrologic setting of the SFVF is the Coconino Plateau, a ~13,000 km^2 area bounded by the Colorado River, the Little Colorado River, and the southwestern margin of the Colorado Plateau. The region surrounding Flagstaff is densely populated by northern Arizona standards, and dependent on several sources for water. The municipal and suburban water supply is derived from surface water (primarily Lake Mary, southeast of Flagstaff), shallow, perched water-bearing zones, and wells drilled into the deep (250-700m) regional aquifer.

The SFVF ranges in elevation from about 1,500 meters to about 3,850 meters. Average annual precipitation over the volcanic field and surrounding terrain ranges from about 60 cm to less than 25cm (Table 3). There are no perennial streams in the area.

Deep canyons bound the volcanic field and the extensive horizontal sedimentary platform on which it is built. The Grand Canyon and the canyon of the Little Colorado River lie to the north, while the valley of the Verde River lies to the south (Figure 5)

Contoured elevations of the surface of the water table define a roughly southeast-northwest axis just south of Flagstaff (Sass et al., 1994; Bills et al., 2000) from which groundwater flows north and south, feeding springs that emerge in the walls of the bounding canyons. Some of these springs are thermal (*e.g.,* see Laney and Brizzee, 2003), which we interpret to reflect heat from a magma/hot-pluton body beneath the SFVF being swept laterally with the regional flow of groundwater.

Throughout the SFVF, siltstones of the Supai Group (Figure 5) tend to act as aquitards to restrict the downward movement of water to the underlying limestones. The unusually large depth to the water table throughout the region explains the ambiguity in interpreting geologic and geophysical indicators of heat at depth, and the absence of the usual surface indicators of hydrothermal activity.

Station Name	Latitude	Longitude	Altitude m	Period of record, years	Average Annual Precip., cm	Mean Annual Temp.°C
Flagstaff Airport	35 08’	111 40’	2,137	107	57.9	7.7
Fort Valley	35 16’	111 45’	2,240	91	57.1	6.2
Grand Canyon NP 2	36 03’	111 09’	2,070	26	48.4	9.2
Munds Park	34 56’	111 38’	1,972	16	no data	8.1
Oak Creek Canyon	34 58’	111 45’	1,548	59	no data	13.3
Sedona	34 52’	111 46’	1,286	57	47.4	15.6
Seligman	35 20’	112 53’	1,600	80	31.9	11.2
Sunset Crater NM	35 22’	111 33’	2,128	33	42.0	7.6
Tuzigoot NM	34 46’	112 02’	1,058	25	37.1	17.4
Wapatki NM	35 41’	111 22’	1,497	57	21.8	14.3
Williams	35 41’	112 11’	2,057	94	53.8	9.9

Table 3. Climate data at and around Sunset Crater. NP = National Park; NM = National Monument.

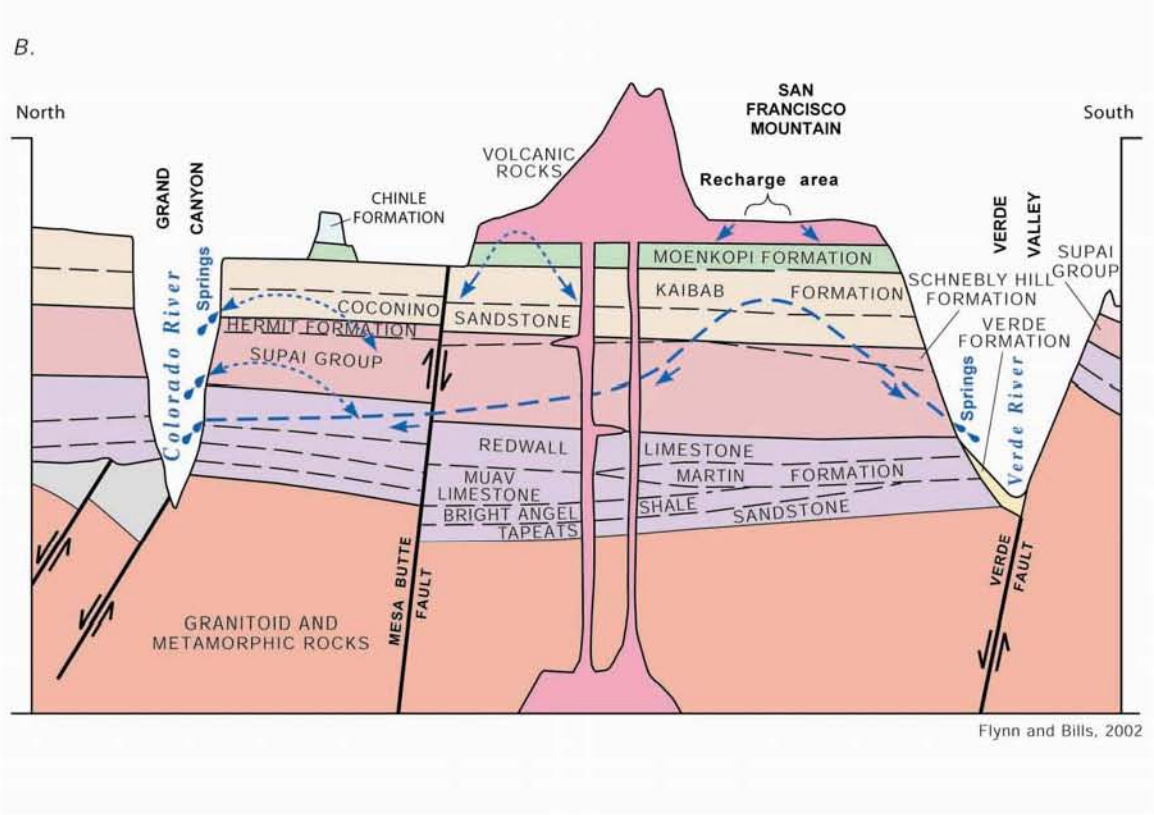

Figure 5. Generalized NNW-SSE Cross section between Grand Canyon and the Verde Valley, showing approximate depth to water (Bills and Flynn, 2002).

THERMAL REGIME

The thermal regime of the southwestern United States generally reflects its Cenozoic tectonic history, with some major overprints attributable to regional hydrology. Most of the terrain comprising the Great Basin, the Southern Basin and Range and the Colorado Plateau margin is characterized by moderately high to high heat flow. Of special note, the Eureka heat-flow low of Nevada (EL, Figure 6) has been interpreted to be the result of regional inter-basin ground-water flow that mines subsurface heat "upstream" and delivers it to the surface "downstream" at hot springs and as evapo-transpiration (Sass et al., 1971).

Viewed in the context of the southwestern United States (Figure 6), heat flow within the SFVF near Flagstaff (Flg, Figure 6) is anomalously low, despite being the site of very young volcanism. As a rule, hydrothermal systems of sufficient size to fuel a geothermal power plant are located within or adjacent to zones of surface heat flow greater than 100 mW m^{-2}. In view of what is known about volcanism in the area, a hydrologic explanation for the observed anomaly must be considered.

When values of heat flow and contours of the ground-water table are mapped together (Figure 7), a hydrologic explanation for the low heat flow in the SFVF seems

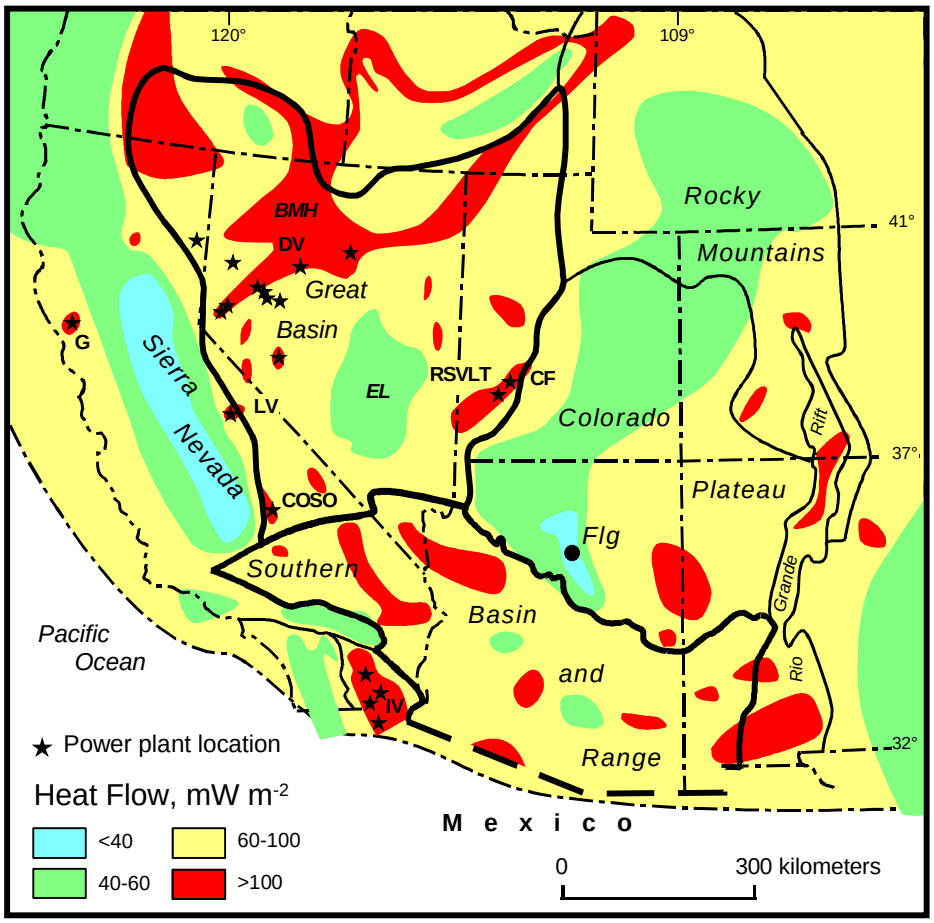

Figure 6. Heat flow distribution in the southwestern United States.

reasonable. Ground water levels are highest just south of Flagstaff, and drop off steeply to the north, beneath the SFVF, including our target area. Thus, ground water flowing northward and downward sweeps much of the heat (that would otherwise be conducted vertically to the surface) laterally to be discharged at springs and seeps along the canyon of the Little Colorado River, and/or dissipating the heat by evapo-transpiration in low-lying areas

Temperature profiles from the wells from which the heat flows were calculated are plotted with common origin in Figure 8. Temperature measurements above the water table can be distinguished from those below it by the density of points on the profile. Temperatures measured in air are typically at 5-10 meter intervals, whereas those in water are much closer together. Heat flow values were calculated from the linear segments of the temperature profiles.

During heat-flow surveys, conductive temperature gradients measured in wells commonly are extrapolated upward to estimate a ground-surface temperature (T_o) undisturbed by diurnal weather cycles and longer-term patterns of climate change. These temperatures (T_o) are then plotted against well-head elevations to determine what is called the lapse rate, which is an indicator of the effect of elevation on temperature. Worldwide,

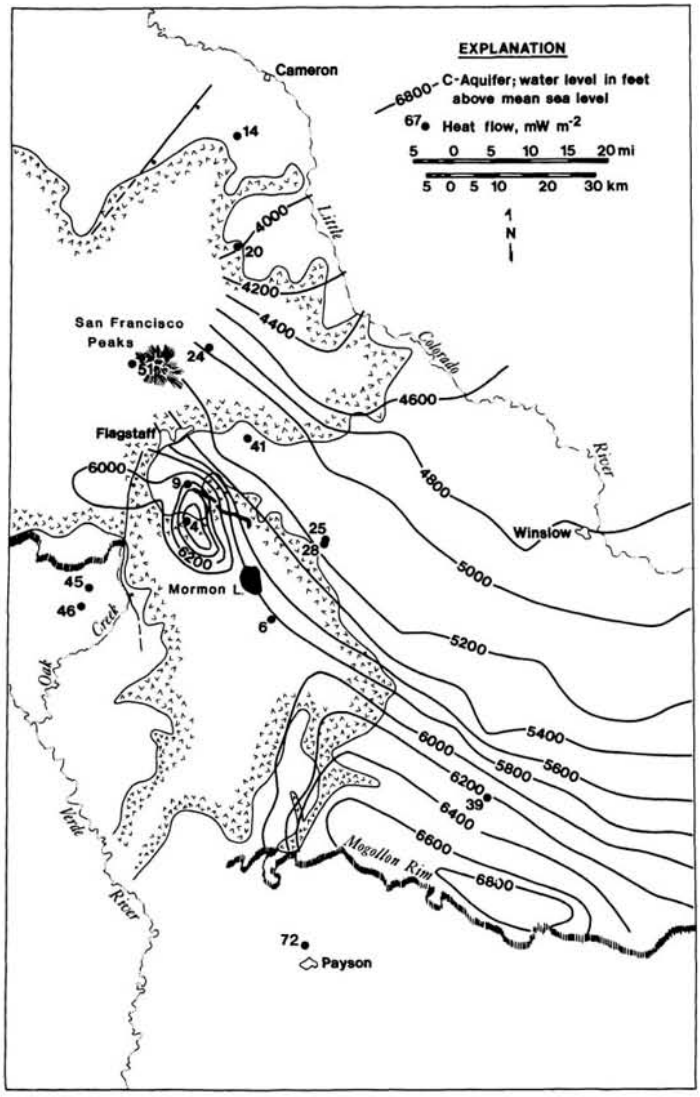

Figure 7. Heat flow and water-level contours for the eastern San Francisco Volcanic Field and adjacent areas (from Sass et al., 1994).

lapse rates generally are in the range of 4 to 6 °C km^{-1}. Sass et al. (1982) have shown that the lapse rate for the SFVF is nearly 12 °C km^{-1} (Figure 9), far greater than the worldwide value. One implication of the SFVF lapse rate is that temperature at sea level and deeper, beneath the volcanic field, is higher than would be expected from a simple downward extrapolation of conductive gradients than would be expected from a simple downward extrapolation of conductive gradients. This implication, in turn, suggests that the near-surface thermal regime within the SFVF is detached from the deep regime. Lateral ground water flow in the regional aquifer is a logical candidate to explain such detachment. Several weather stations are located in the SFVF and the immediately surrounding region. Surface air temperature records have been kept at 11 of these stations (Table 3) for a period

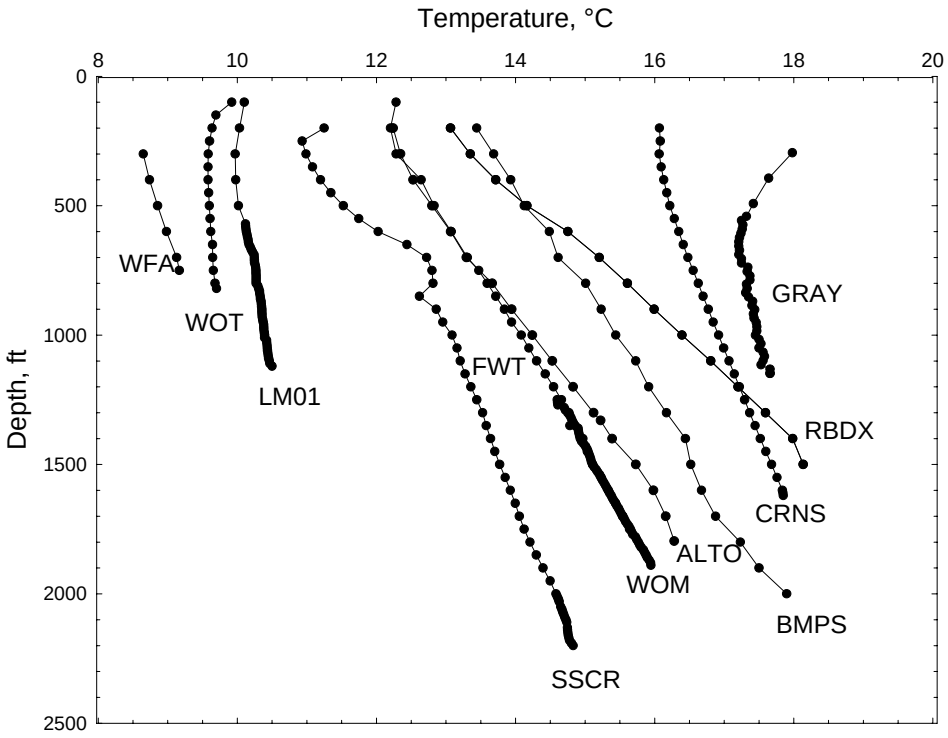

Figure 8. Temperature Profiles from observation wells in the SFVF.

.

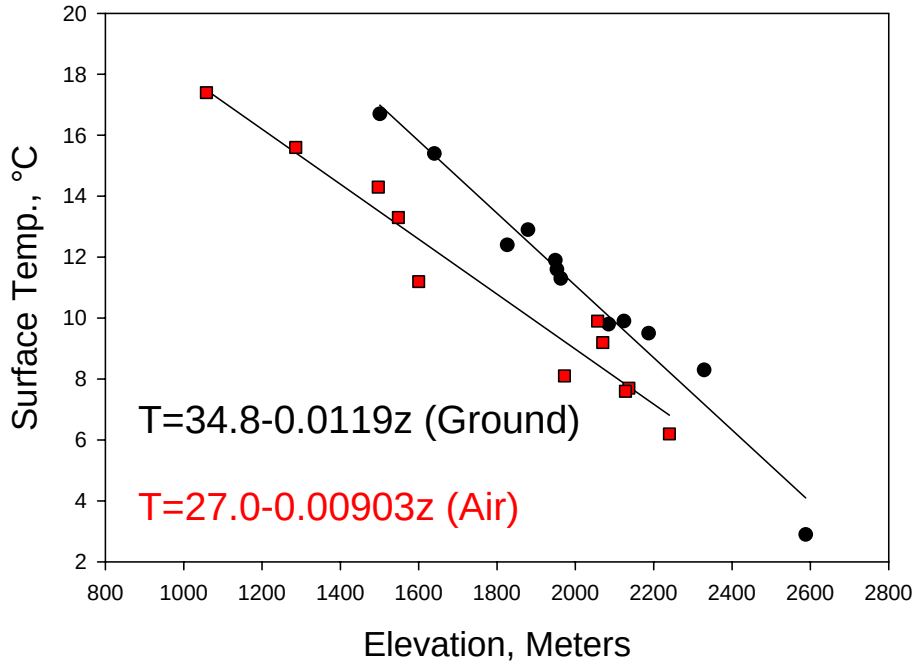

Figure 9. Air and Ground temperatures as a function of elevation for SFVF.

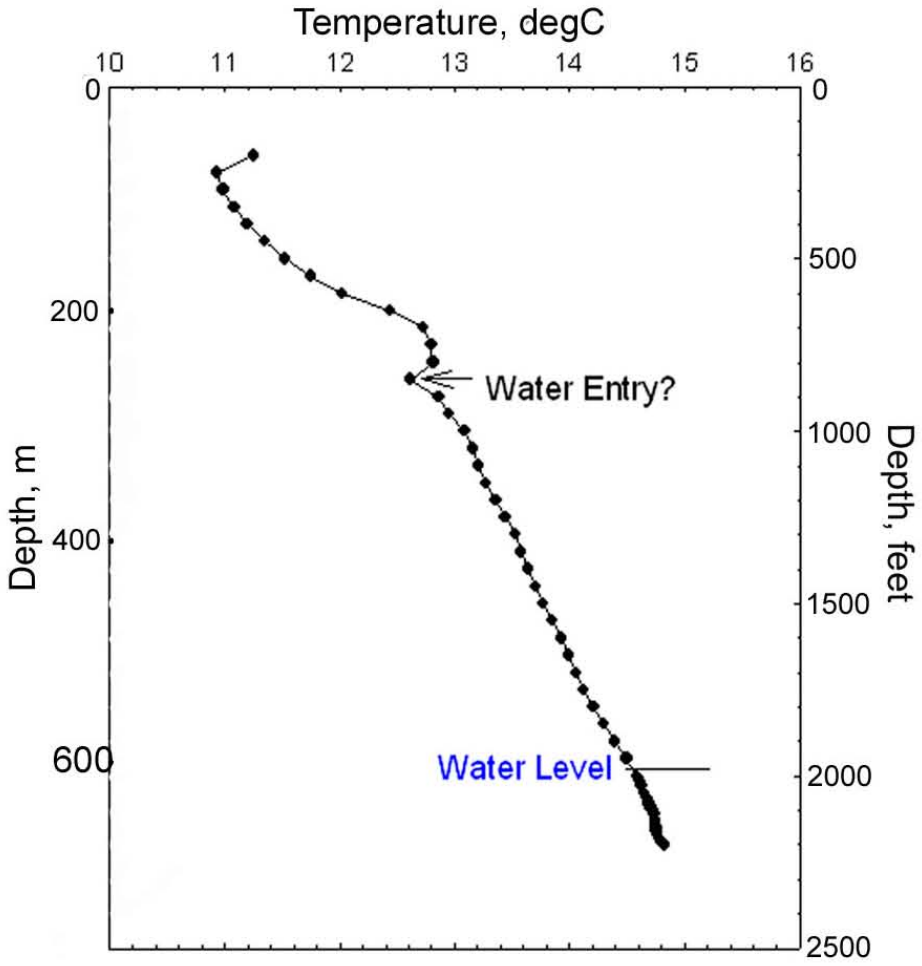

Figure 10. Temperature Profile for SSC-1, near Sunset Crater

sufficient to establish a reliable mean. These temperatures are also plotted as a comparison with those extrapolated from the temperature profiles. The lapse rate in air is still higher than the world average, but 25% lower than that from ground temperatures. The observation that air temperatures are cooler than ground temperatures is consistent with data from other regions, but the difference in slopes supports our hypothesis of the shallow thermal regime being decoupled from that at depth. The temperature profile of well SSC-1 (Figure 10) is consistent with others that have been measured in the SFVF (see Figure 8). The average thermal gradient is low, and there is no sharp temperature discontinuity at the water table. The thermal gradient below the water table is somewhat lower than that above, and the temperature-depth profile is slightly concave-upwards near the bottom of the well, indicating downward water flow. The mean heat flow from SSC-1 is 24 mW m^{-2}, hardly indicative of a geothermal resource under ordinary conditions.

Implications of Thermal Observations

During the Exploration boom of the late 1970s, the SFVF was the object of reconnaissance exploration by several energy companies. The absence of near-surface geothermal manifestations and the low temperatures in observation wells were naturally viewed as negative indicators, despite the presence of large and relatively young silicic bodies, and the very young (< 1,000y) basaltic volcanism at Sunset Crater. The expense of deep boreholes necessary to resolve the apparent contradiction had to be weighed against the availability of more promising targets elsewhere. Stauber's (1982) interpretation of the seismic P-delay anomalies observed beneath the SFVF suggests an average geothermal gradient in the upper crust on the order of 100 °C km^{-1}, in contrast to the 0-10 °C km^{-1} from the shallow wells studied. A possibility of temperatures in the range of 250°C at economically drillable depths, not counting residual heat from young volcanic activity, if the postulated zone of thermal decoupling is fairly shallow (~1 km or so).

Of critical importance to our assessment of geothermal potential of the Sunset Crater area is the nature of the interface between the regional aquifer and deeper rocks. If pervasive vertical penetration of groundwater has occurred or exists into the deep section of Paleozoic rocks and underlying Precambrian crystalline rocks, then it is likely that most of the heat associated with Holocene volcanism has been dissipated. On the other hand, if the lower boundary of the regional aquifer is impermeable as suggested by recent hydrologic studies (Bills et al., 2000), then cooling of magma reservoirs would be by conduction, and sufficiently high temperatures for the generation of electricity might be present.

GROUNDWATER CHEMISTRY

Heat flow data from the San Francisco Volcanic Field are not typical of a geothermal system because heat is stripped from the uppermost crust by the infiltration of meteoric waters (Sass et al., 1994). Similarly, the field is devoid of hydrothermal manifestations, in fact, any springs are rare except those fed by snow melt around the mountains. However, there are numerous groundwater wells in the area and the chemistry of the waters in these wells has been studied by Taylor (1997) as geothermometers. Geothermometers assume that the groundwater is not stagnant and that its chemistry is dominated by the highest temperature that it attains while flowing underground. Using experimental systems, geothermometers have been calibrated for temperature, and the primary system that will be considered here is the silica geothermometer, which depends on the temperature-dependent solubility of SiO_2 in water. Two factors must be considered when interpreting groundwater geothermometer data: (i) the well where the data are collected may not be the location where the groundwater attained its maximum temperature; and (ii) groundwaters may mix, and groundwater chemistry may re-equilibrate to lower temperatures, so maximum temperatures may be underestimated. Using a technique to estimate heat flow from groundwater silica concentrations, Swanberg and Morgan (1979, 1985) estimated the average heat flow from the eastern San Francisco volcanic field to be about 75 mW m^{-2}.

Taylor (1997) studied groundwater data from wells within a rectangular region between longitudes 111° 00' and 112° 30' W and latitudes 34° 15' and 36° 15' N, and in

this region there were 544 silica analyses. A new contour map of the silica geotemperatures using data up to and including 2003 has been calculated and is shown in Figure 11. This map shows silica geotemperatures in excess of 80°C around the San Francisco Peaks. High silica geotemperatures are also shown in the Verde Valley to the south where groundwaters from the San Francisco Peaks discharge. These data are therefore further data for high subsurface temperatures in the San Francisco volcanic field. Unfortunately there are no wells in the target area for analysis, but the trend the contours of these data suggest that the high silica geotemperatures continue into this region.

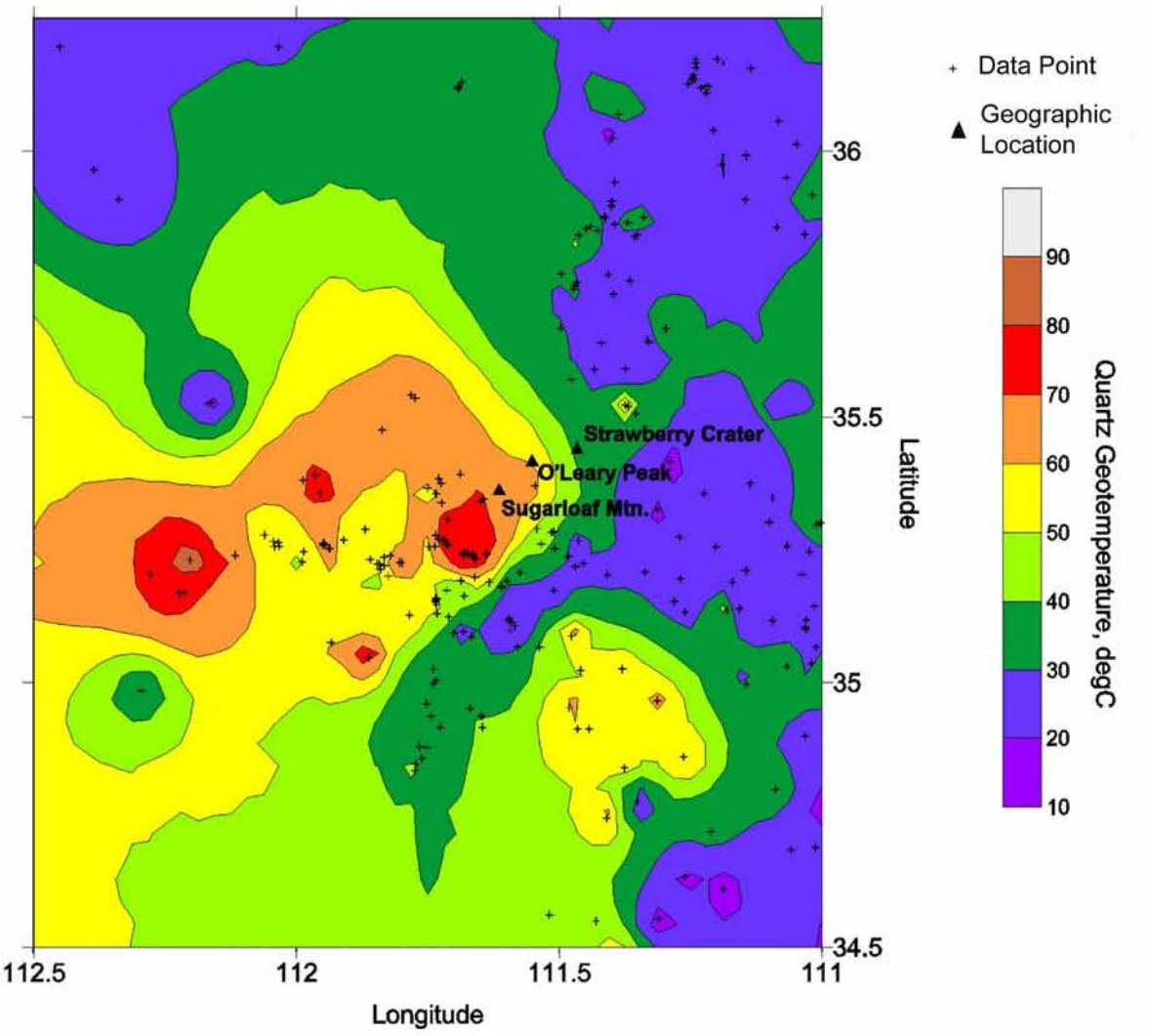

Figure 11. Silica geotemperature contour map of San Francisco Volcanic Field and surrounding regions. Contour interval is 10°C.

SEISMIC AND ELECTROMAGNETIC STUDIES

Additional evidence for residual heat in the crust beneath the eastern portion of the San Francisco Volcanic Field has been derived from seismic data. Stauber (1982) analyzed data from distant earthquakes recorded on a northwest-southeast line of seismographs across San Francisco Mountain (Figure 12). These data indicated significant delays for ray-paths traveling through the crust beneath San Francisco Mountain, which Stauber (1982) interpreted to indicate a low-velocity body in the crust approximately 6 km wide at depths between 9 and 34 km below sea level below sea level (Figure 13). The decrease in velocity in this body was more than 6% with respect to the surrounding rocks, and this result is consistent with partially molten and/or anomalously hot rock in the mid to lower crust.

A more recent, shallow seismic study detected what has been interpreted to be the upward extension of this hot body into the upper crust (Durrani et al., 1999). This experiment used explosive sources shooting side shots ("fan shooting") into linear arrays of receivers and the primary phase recorded was the upper crustal arrival (*Pg*) so that the study was sampling the upper 5 km. The seismic-velocity image obtained indicated a high-velocity zone at upper crustal depths beneath the San Francisco Mountain, with *P*-wave

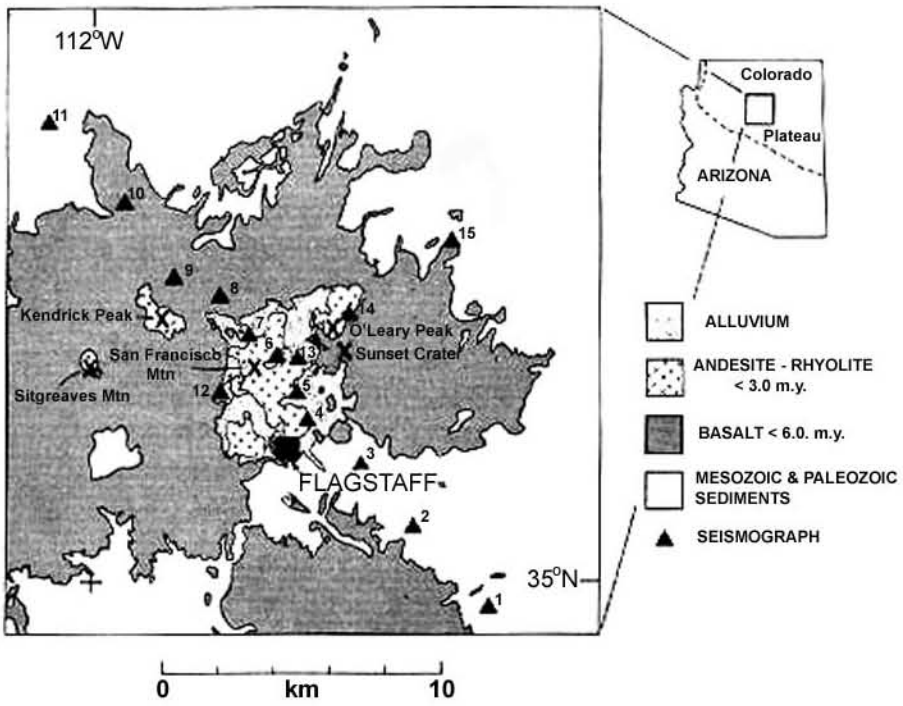

Figure 12. Locations of seismographs used to record teleseismic arrivals for teleseismic P-wave residual analysis by Stauber (1982; from Stauber, 1982).

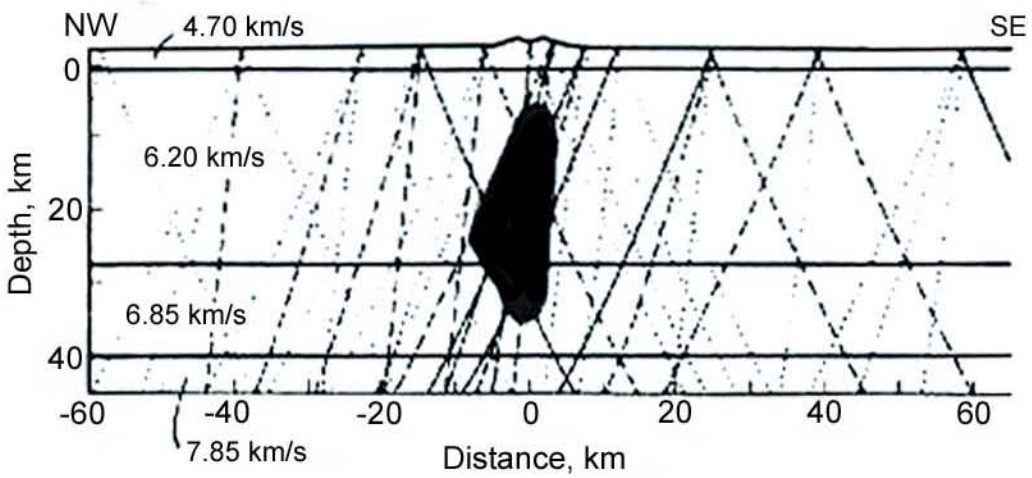

Figure 13. Cross-section showing ray-paths for 28 events recorded along the profile and the interpreted low-velocity body in the profile [from Stauber, 1982].

velocities 6% higher than the surrounding basement rocks (Durrani et al., 1999). This high-velocity zone appeared to lie immediately above the low-velocity middle and lower crustal body of Stauber (1982). Durrani et al. (1999) suggest that they could be the same body, the inversion in velocity contrast perhaps resulting from cooling upward within the body and compositional changes in the host rock. At depth the body is hotter, has a higher percentage of partial melt, and is more silicic than its host rock, resulting in a negative velocity contrast. At shallow depths the body is not so hot, has little or no partial melt, and is more mafic than its host rock, resulting in a positive velocity contrast. Unfortunately, none of the ray paths in this study crossed in the region between San Francisco Mountain and O'Leary Peak, the target area indicated to be the area with the highest geothermal potential from the geologic and age-dating data. The upper-crustal velocity body does appear to end abruptly in this direction (Figure 5 of Durrani et al., 1999), but neither the Stauber (1982) study nor Durrani et al. (1999) give good constraints on seismic velocities beneath the target area.

Geomagnetic variation studies, a forerunner of magnetotelluric studies, across the San Francisco Volcanic Field have detected an anomalous geomagnetic variation field in the vicinity of the San Francisco Peaks (Towle, 1984). This anomalous field was interpreted by Towle (1984) to be caused by a regional telluric current system flowing parallel to the Mesa Butte and Bright Angel fault systems as described by Shoemaker et al. (1978), and shallow portions of this local telluric current concentration were reported to be at a depth of no more than 10 km. Towle (1984) concludes that the high electrical conductivity associated with the geomagnetic anomaly could be associated with high temperature remnants associated with the San Francisco Volcanic Field. Additionally, Towle (1984) concludes that further studies would be necessary to study the relation between the geomagnetic variation anomaly and the low seismic velocity anomaly of Stauber (1982) beneath San Francisco Mountain. Unfortunately no such further studies were made, and none of Towle's (1984) geomagnetic recording stations were particularly close (< 15 km) to the target area. In conclusion, the geomagnetic variation studies give good evidence on a regional scale consistent with high temperatures in the crust, but no local data are available.

GRAVITY AND MAGNETIC STUDIES

Gravity and magnetic studies of the San Francisco Volcanic Field have been published by Mickus and Durrani (1996). These data have were interpreted to be basically consistent with both the shallow and deep crustal seismic studies, but also show additional upper to mid crustal bodies (Mickus and Durrani, 1996) These upper and mid crustal bodies were interpreted to be a mixture of ages ranging from Precambrian to Recent, the youngest bodies being associated with the San Francisco volcanics.

Additional gravity data were collected inside and within ten-miles of the boundary of the target area, and these data were combined with the raw gravity data set used by Mickus and Durrani (1996) which was kindly provided to us by Professor G. R. Keller of the University of Texas at El Paso. The Bouguer gravity anomaly data from the combined data set are shown in Figure 14. A topographic correction was then applied to these data using a digital terrain model from the U. S. Geological survey and software in the commercial program Oasis Motaj v5.1 (Geosoft Inc.), and the resulting terrain corrected complete Bouguer gravity anomaly data are shown in Figure 15.

Two and a half dimensional (2½ D) gravity models were developed to match the complete Bouguer gravity data along profiles that were approximately perpendicular to the strike of the anomalies (2½ D gravity models are models constructed using horizontal prisms of limited length perpendicular to the profile that is being measured and with the profile located over the center of the prisms). Five profiles were modeled and their locations are shown in Figure 16. The results of these modeling exercises are shown in Figures 17 though 21, each of which shown the final model, the complete Bouguer gravity data and modeled gravity along the profiles.

The uppermost layer in each profile (above zero km and shown in yellow) is the Phanerozoic sedimentary section and as it is constant in thickness is causes no variations in the gravity anomalies. Some short-wavelength gravity anomalies required low-density bodies immediately below this sedimentary section (also shown in yellow or grey), and these bodies are also thought to be sedimentary in origin, either Phanerozoic in age, of perhaps part of the Late Proterozoic Grand Canyon Supergroup which is exposed in the Canyon, and identified as GCSG on some profiles where the shape of the bodies resembles the faulted dipping attitude of these sedimentary rocks.

In the discussion below, all depths are given below sea level; for approximate depths below the surface add 2 km. In figures 17 through 21, large bodies below zero km are colored orange if they have a negative density contrast and green if they have a positive density contrast.

Profiles A-A’ and B-B’ have large bodies with positive density contrasts either where they come closest to, or where they cross the San Francisco Peaks (Figures 17 and 18). These bodies correspond to the large lower, middle and upper crustal seismic anomalies, and are consistent with extensive mafic intrusion into the crust generating the intermediate and felsic magmas that have erupted during the part million years or so in the San Francisco Peaks.

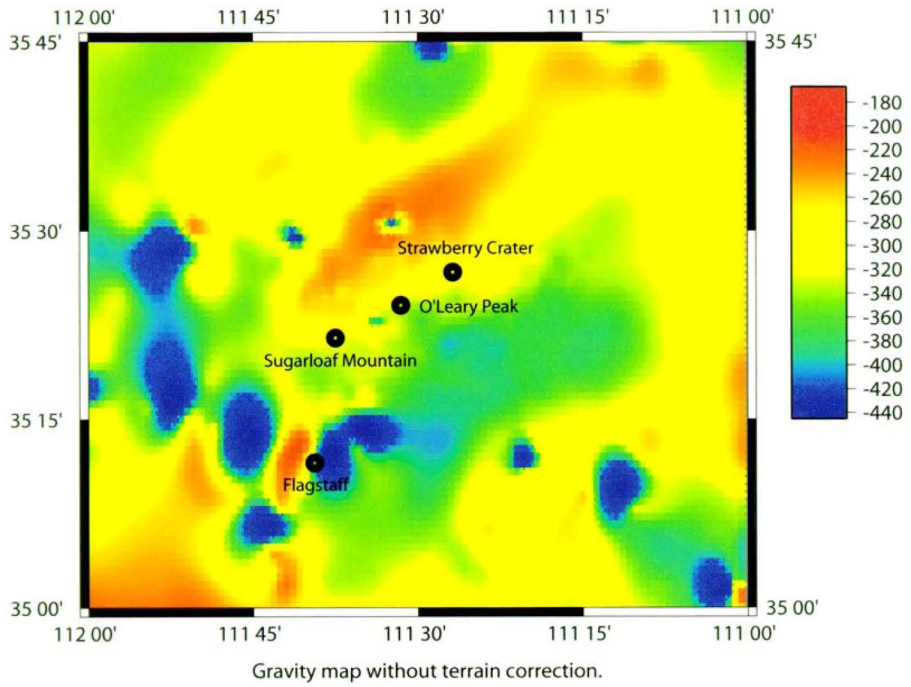

Figure 14. Simple Bouguer gravity map (without terrain corrections) of study region. Anomalies are in mGal.

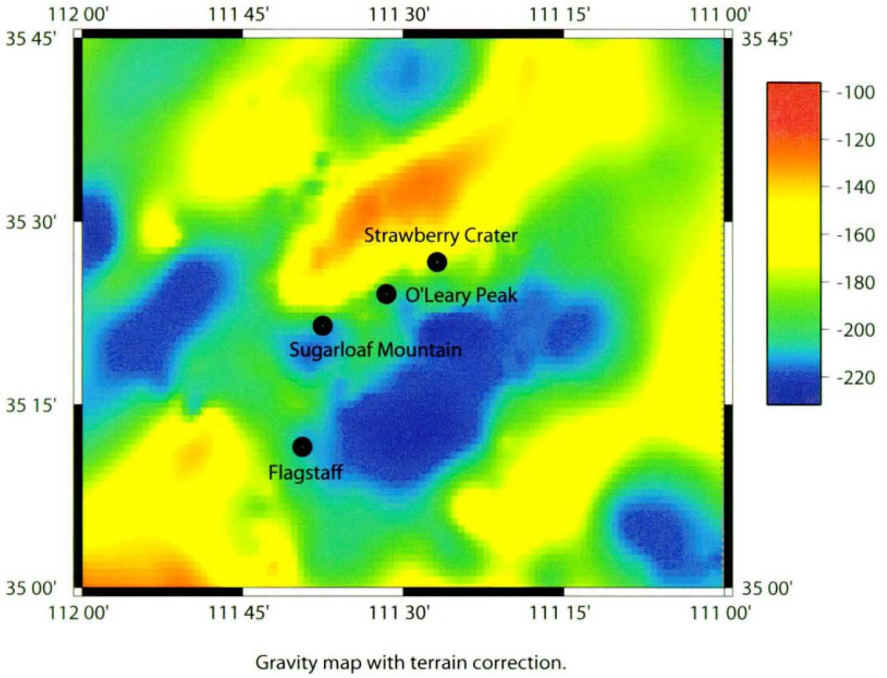

Figure 15. Complete Bouguer gravity map (with terrain corrections) of study area. Anomalies are in mGal.

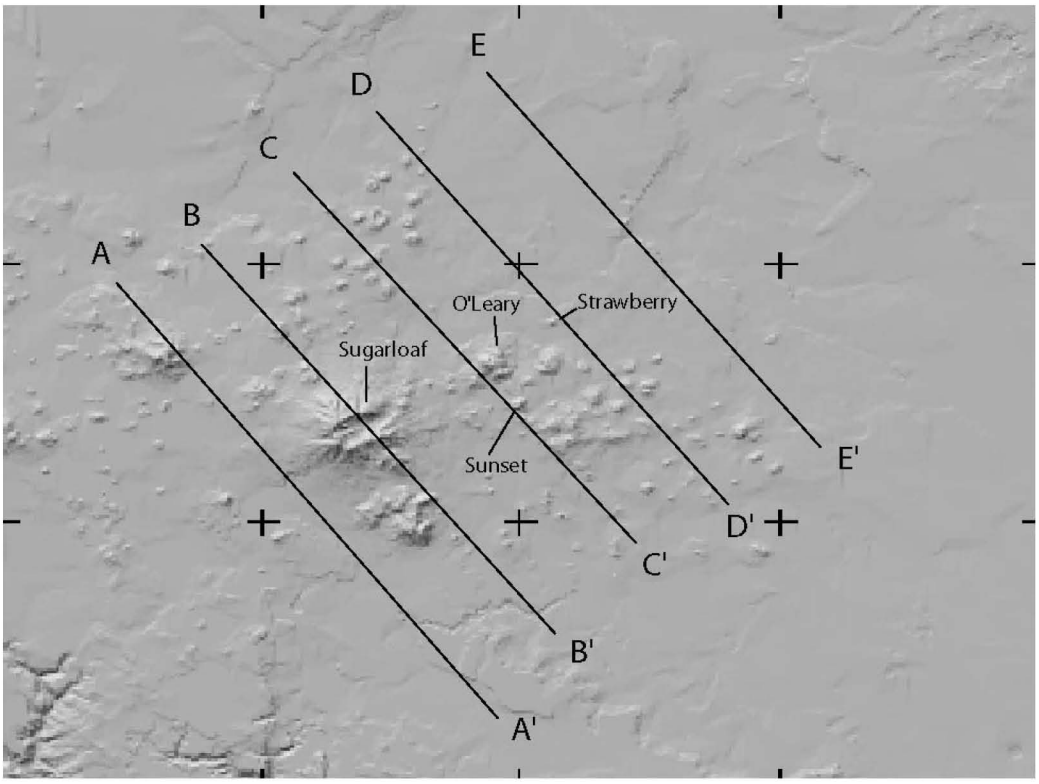

Figure 16. Digital terrain model of study area showing locations of gravity model profiles. The area shown in this map is the same as that shown in Figures 14 and 15. The tick marks and plus signs are latitude and longitude markers.

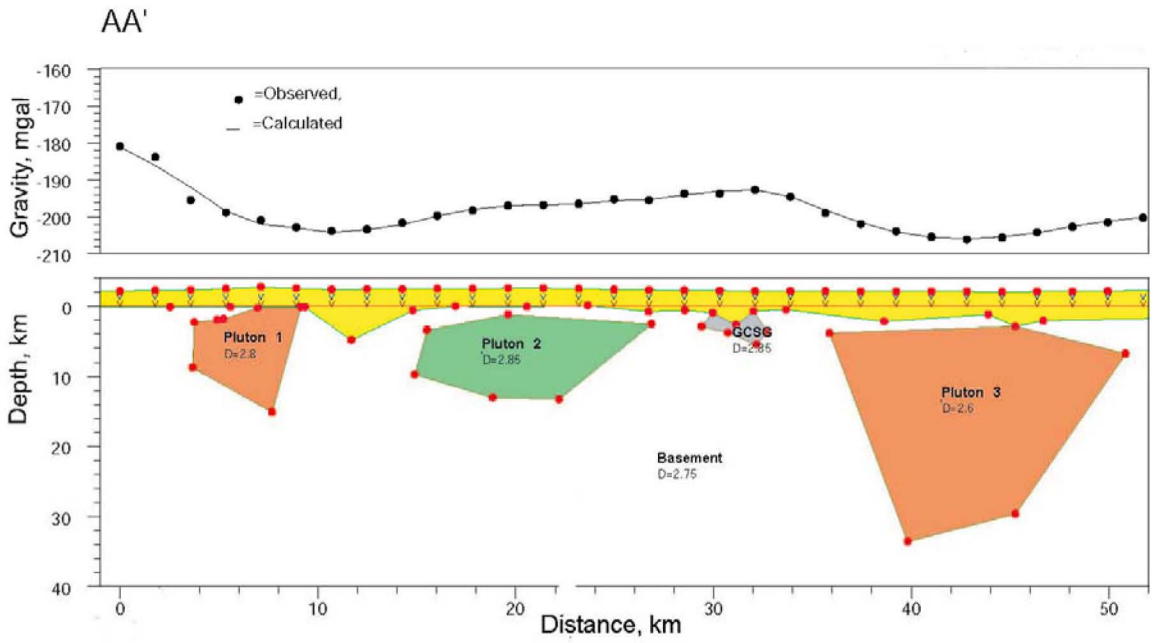

Figure 17. Gravity model for profile A-A'. See text for discussion.

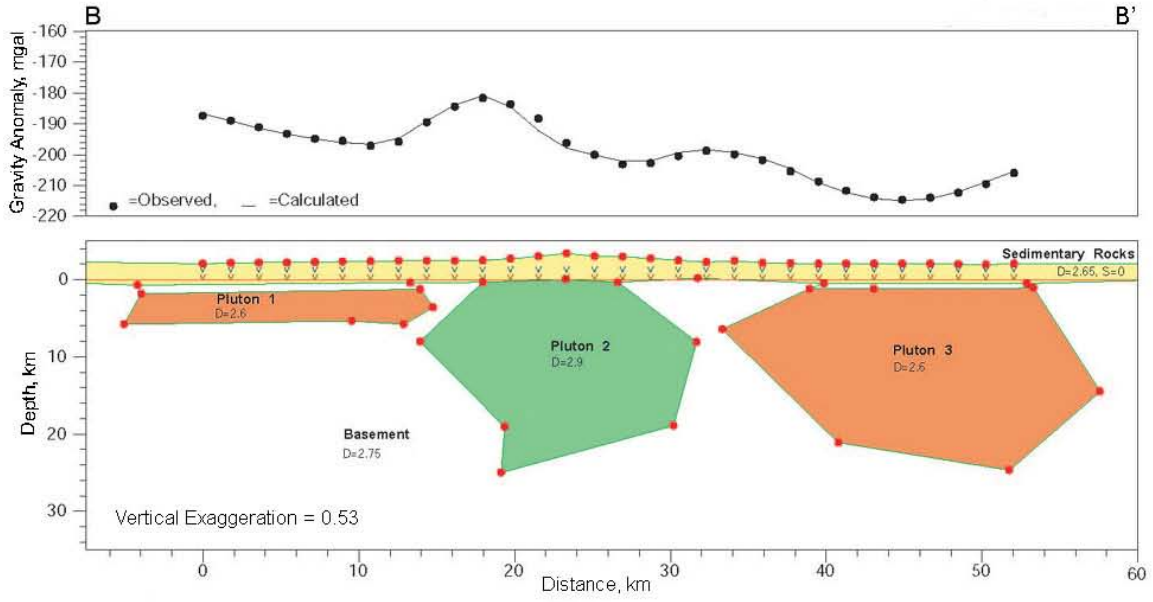

Figure 18. Gravity model for profile B-B'. See text for discussion.

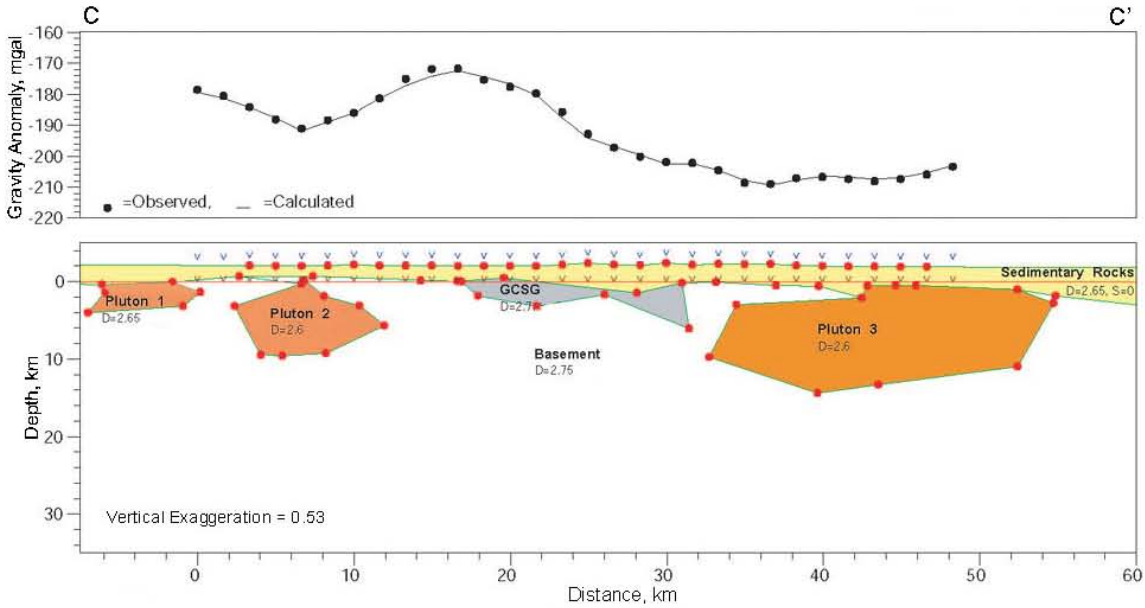

Figure 19. Gravity model for profile C-C'. See text for discussion.

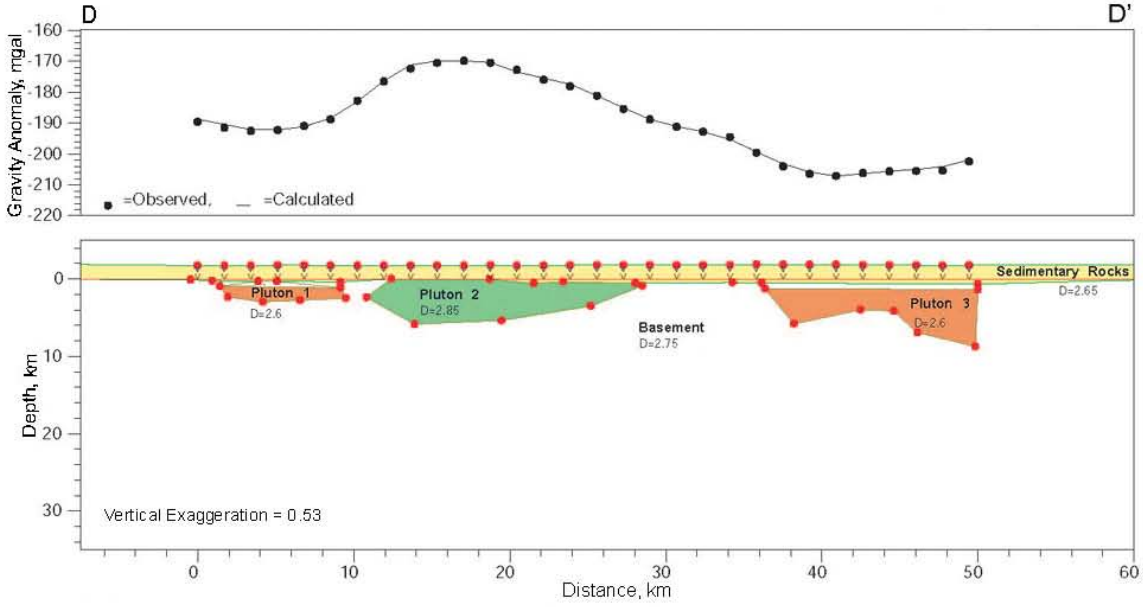

Figure 20. Gravity model for profile D-D'. See text for discussion.

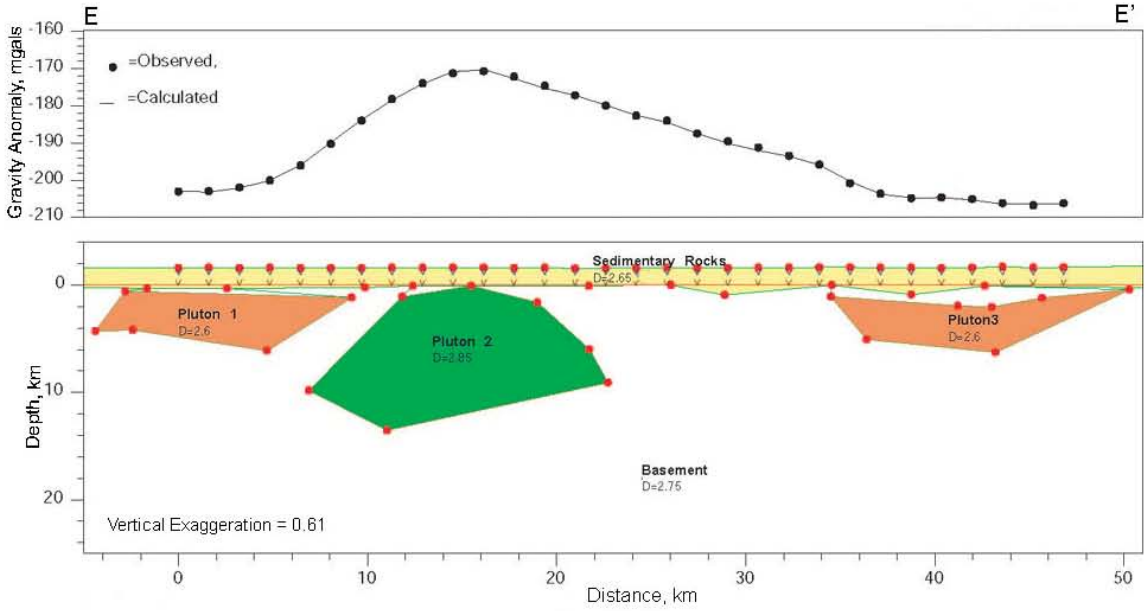

Figure 21. Gravity model for profile E-E'. See text for discussion.

A second dense body underlies the north end of profile A-A' (Figure 17), which underlies Kendrick Peak, a smaller and older volcano than the San Francisco Peaks. This dense body is interpreted as an intrusion associated with Kendrick Peak. Near the north end of profile B-B' a thin, low density body extends from about 2 km to 6 km below sea level and extends about 20 km along the profile (Figure 18). On profile C-C' two low density bodies were modeled beneath the northern half of the profile (Figure 19). The southerly of these bodies is probably a lateral extension of the northern body on profile B-B', but it is reduced in length along profile to about 10 km and increases in thickness to 10 km. The same body appears to continue over to the northern end of profile D-D' (Figure 20). This body underlies a field of basaltic lava flows and cinder cones north of the San Francisco Peaks (Figure 16), the youngest of which is SP crater with an eruption date of about 17,000 years BP. A smaller low density body was also modeled extending to about 2 km depth immediately north of the 10 km body on profile C-C' (Figure 19).

A very large low density body was modeled near the south end of profile A-A', extending over 10 km along the profile and to about 30 km in depth. A similar body was picked up near the south ends of profiles B-B' and C-C', but is broadened to over 20 km along both of these profiles and shallowed to about 25 km on profile B-B' and 15 km on profile C-C'. The same body may also be continuous as a thin, low density body near the south ends of profiles D-D' and E-E', where it only extends to a maximum of about 8 km (Figures 20 and 21).

Immediately south of the low density bodies at the north ends of profiles D-D' and E-E', high density bodies were modeled in the upper crust. The body on profile D-D' extends about 18 km along the profile and down to a depth of 5 km (Figure 20) and the body on profile E-E' extends about 16 km along the profile and down to a depth of 13 km. These bodies are probably one and the same body, but there is no young (< 5 Ma) surface volcanic activity that immediately overlies this body, suggesting that it is not related to volcanism of the San Francisco Volcanic Field.

A map view of the modeled gravity bodies with interpreted connections of the bodies between the profiles is shown in Figure 22. These model bodies are superimposed on the digital topography model for the area. Strong arguments relating the bodies modeled from the gravity data to topographic expression of magmatic activity in the San Francisco Volcanic Field cannot be made. The problem with interpretation of the gravity data is that there are at least two sources for the gravity anomalies: (i) anomalies associated with Proterozoic events that affected the crust of the Southwestern US from its addition to cratonic North America from 1.8 through 1.4 Ga through its stabilization in the Paleoproterozoic; and (ii) anomalies associated with the emplacement of the San Francisco Volcanic Field. The requirement of bodies with both positive and negative density contrasts to model the gravity anomalies also leaves the possibility that there may be complementary pairs of bodies with opposite density contrasts that cancel each other out in terms of gravity anomalies. Thus, the absence of modeled gravity bodies beneath areas of surface volcanism cannot be taken as an indication of a lack of density anomalies in the crust beneath these surface manifestations, only that they are not required by the gravity data. The youngest magmatic activity, in fact, may have been focused between older magmatic bodies.

In summary, the gravity data indicate that there are an abundance of upper crustal density anomalies that are consistent with plutonic activity of the type that heats

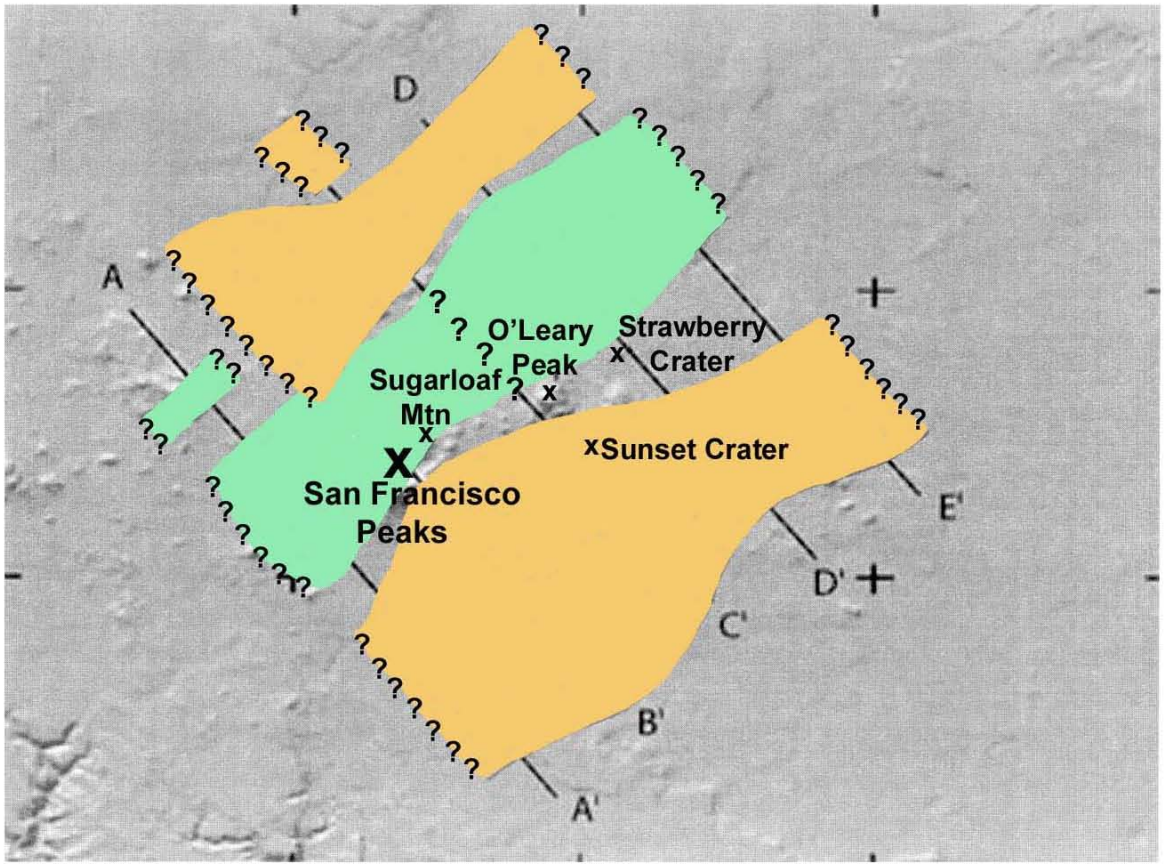

Figure 22. Map view of the modeled gravity bodies with interpreted connections of the bodies between the profiles. Denser bodies are shown in green; lower density bodies are shown in orange. Area is same as shown in Figures 14, 15, and 16. Background is the digital topography of the area.

geothermal reservoirs. However, gravity alone cannot determine the age of these bodies, and there is certainly a mix of ages beneath the San Francisco Volcanic Field, dominated by Proterozoic age plutons and much younger plutons associated with the volcanism of the volcanic field.

OTHER STUDIES

As this study was coming to completion we were made aware of independent studies of travertine deposits and strings in the Grand Canyon to the north of the San Francisco Volcanic Field by Laura J. Crossey at the University of New Mexico and co-workers. Preliminary results of this work have been submitted for publication (Crossey et al., 2004), but their results strongly confirm our conclusions of a two layer hydrothermal system in the San Francisco Volcanic Field, with a shallow system masking a deeper geothermal system. The results of the Crossey et al. (2004) study are summarized in Figure 23. They found a component of volcanic gasses in the deeper waters, giving evidence for recent geothermal waters of the type that we have concluded underlie the field.

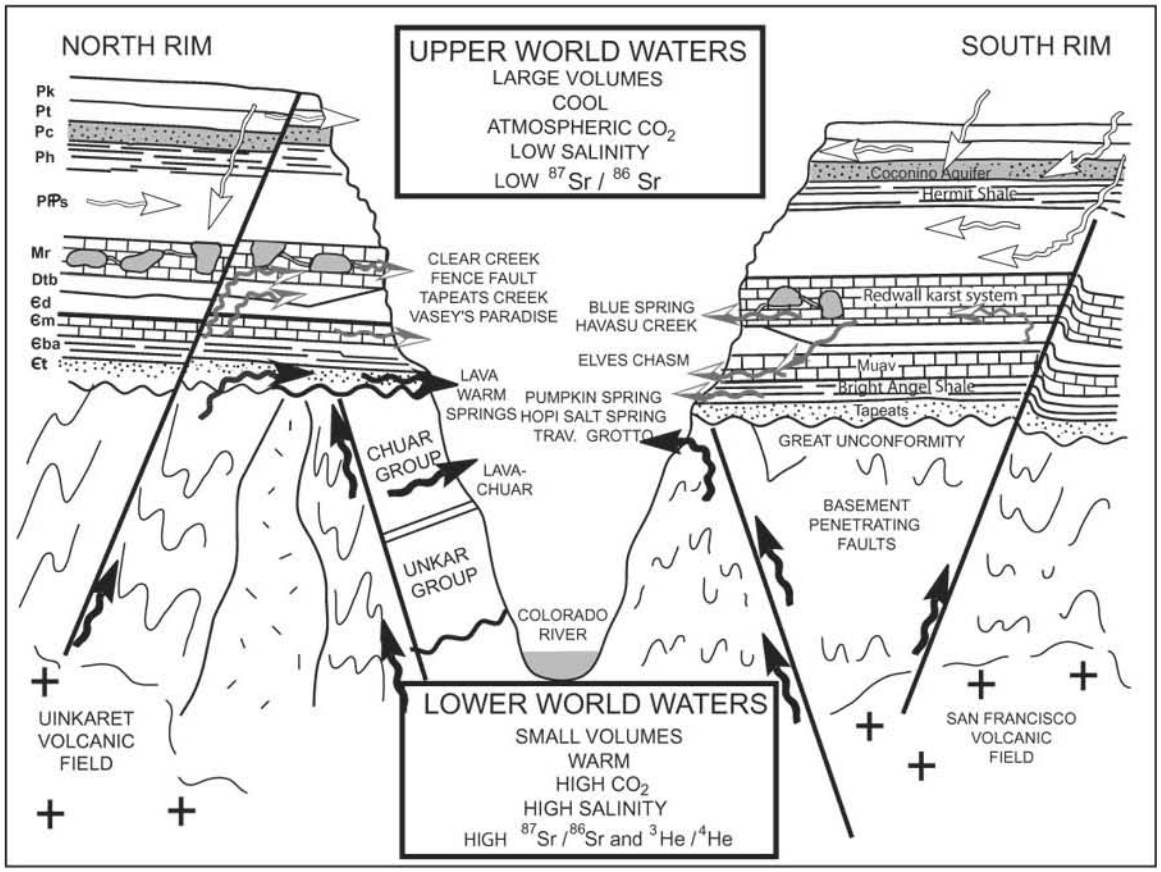

Figure 23. Diagrammatic cross-section of the Grand Canyon north of the San Francisco Volcanic Field showing "Lower World Waters" which have a component of volcanic gases from the San Francisco Volcanic Field on the southern side of the canyon (from Crossey et al., with permission).

SUMMARY

The collection and analysis of new data and the reanalysis of existing data in this study have confirmed that the region to the immediately north of Sunset crater in the San Francisco Volcanic Field in northern Arizona has the potential to be a region of deep elevated geothermal gradients, masked at the surface by groundwater recharge. This interpretation is specifically supported by the geologic mapping and the new age dates of the silicic igneous bodies, both the shallow and deep seismic data, the apparent shift in the extrapolated surface temperatures from the geothermal gradient data, the groundwater silica geotemperatures, and the high CO_2, high salinity, high $^{87}Sr/^{86}Sr$ and high $^{3}He/^{4}He$ waters collected by Crossey et al. (2004) in the Grand Canyon. Unfortunately the gravity data cannot distinguish among Precambrian and younger plutonic bodies in the upper crust, but the strong north-east trend mapped in the geology and followed by the trend of the youngest silicic volcanic bodies is clearly evident in both the gravity and magnetic data sets.

2. CONCEPTUAL MODEL

In the absence of detailed sub-surface information with which to constrain models for the hydrothermal regime at depth beneath our study area, there is wide latitude for speculation on the possible existence of a hydrothermal resource. We shall present some simple, limiting cases, but confirmation of a resource will ultimately depend on drilling at least one well into the Precambrian basement rocks.

Such a well, drilled from Robinson Crater rhyolite dome (RBMT, Figure 24) would traverse Cenozoic volcanic rocks, possibly some Moenkopi formation of Triassic age, and the complete Paleozoic section. Then from a depth of about 1 km, the well would penetrate Precambrian rocks within which we would expect to find a reservoir if one exists. Based on the geologic log of the Sunset Crater well (SSCR), the Supai Group, the lower part of which we assume to be impermeable, would be encountered at a depth of about 600 meters. The observed lack of productivity of the SSCR well at total depth of 670 m suggests that this might be the approximate depth below which temperatures are unaffected by the recharge and lateral flow of the deep regional aquifer depicted in Figure 5. Below this zone of disturbance, the regional temperature gradient will be re-established within a few time

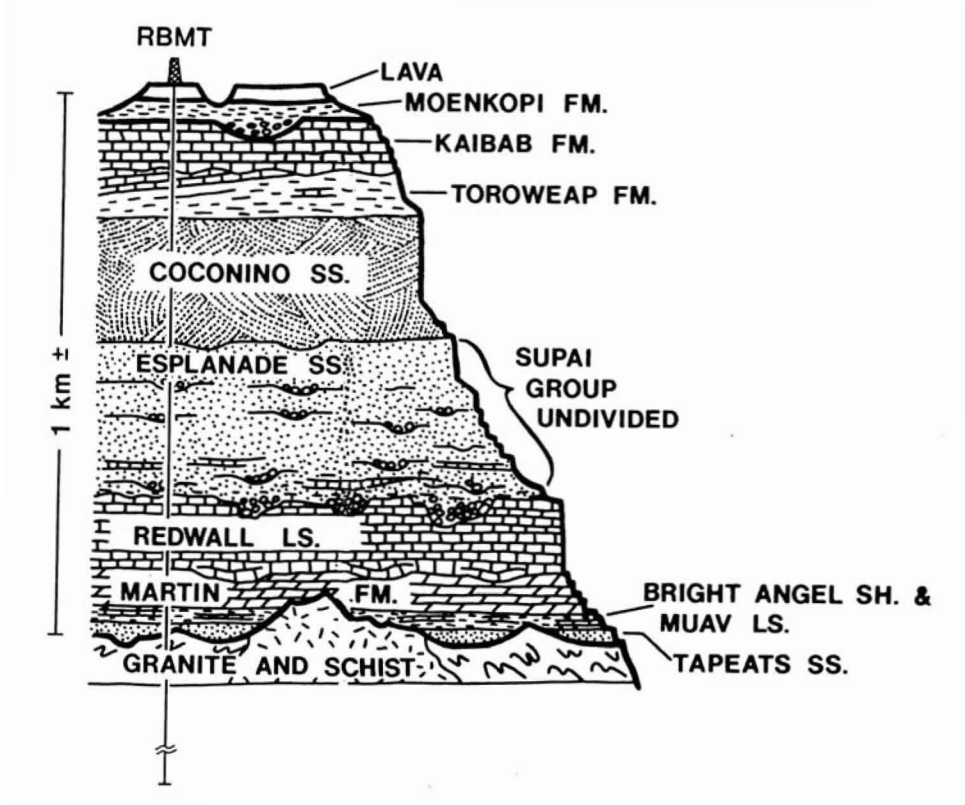

Figure 24. Interpreted Geologic Section beneath the study area showing trajectory of an exploratory drill hole.

constants of the onset of the disturbance. For the sedimentary rocks comprising most of this zone, the average thermal diffusivity is about 0.012 $cm^2 s^{-1}$, and the corresponding time constant for a layer 1 km thick, about 5,000 years. Thus, we can reasonably assume thermal equilibrium for the temperature gradient below the Supai Group and ignore for the moment possible temperature enhancements from upper crustal igneous activity. The average temperature gradient of 100 °C km^{-1} inferred from the evidence for molten rock at 10 km or so (Stauber, 1982) would not be expected in the upper few kilometers, especially when viewed in the light of the Pleistocene volcanic and tectonic history of the SFVF, the current lack of volcanic activity, the absence of significant seismic activity, and the lack of any obvious hydrothermal manifestations. Gradients of this magnitude are associated with vigorous hydrothermal systems like The Geysers, and the Coso volcanic field. They result in near surface conductive heat flow > 200 mW m^{-2} , and combined conductive/advective fluxes >400 mW m^{-2}. We would expect heat flow below the base of the regional aquifer to be more in the range of 100 to 120 mW m^{-2} based on analogous settings elsewhere without the large hydraulic gradients and deep water tables. Assuming a reasonable average upper crustal thermal conductivity of 2.2 W $m^{-1} K^{-1}$, this heat flow corresponds to a temperature gradient of about 50 °C km^{-1}. From these numbers, we can estimate the temperatures at the depths to which we could drill economically, which in today's market is in the range of 2.5 km to 3 km (8,000-10,000 ft). We show two curves (Figure 24), the red curve having the base of the permeable layer at 670 m (the bottom of SSCR) and the other, at 1,000 m, roughly the base of the Paleozoic sediments. Subject to the assumption of a regional temperature gradient of 50 °C km^{-1} beneath the eastern SFVF, temperatures between 2.5 and 3.0 km depths are in the range 90-130°C without calling upon additional heat from youthful magmatism. This temperature range is below that required for flash steam power plants. If large volumes of water could be produced, a reservoir at these temperatures might support a binary fluid power plant, but the economics of such a low-temperature operation would be marginal with current technology.

About 40% of our study area is covered with dacitic and rhyolitic lavas, erupted from vents within the area. Total volume of lavas is about 7 km^3. Additional Rhyolite is found immediately southwest of our area. According to the most recent and reliable geochronology, their ages range from about 90,000 to 270,000 years. Depth, thickness, and volumes of their source magma reservoirs are all speculative. It is thus, impossible to quantify the amount of heat remaining in the magma chambers, and their contribution to any hydrothermal systems that may be reachable by the drill. If we assume effective depths of between 5 and 7 km for the magma chambers, the conductive thermal time constants are between 100,000 and 250,000 years, respectively (see Figure 9 of Lachenbruch and Sass, 1977). The implication here is that even under ideal conditions (large volume compared to surface expressions and heat loss entirely by conduction), a large proportion of the heat will have been lost. The lateral cooling of smaller bodies coupled with hydrothermal convection, for which there is evidence in the water geochemistry, would imply that the present-day temperature anomalies associated with the magma chambers are fairly modest. Without additional subsurface information, we cannot predict temperatures with any certainty, but we can perform a simple calculation to give an order of magnitude.

For the purposes of illustration, we will employ model IIa of Lachenbruch et al. (1976), a square prism, as our hypothetical magma chamber. Assuming that the prism is 6

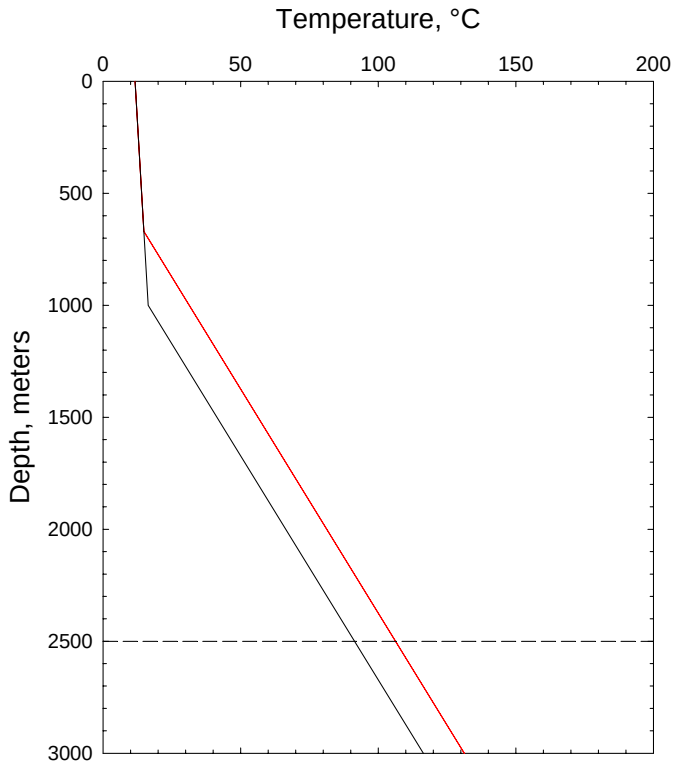

Figure 25. Idealized temperature profiles to 3,000 m near Sunset Crater.

km on a side, with its top at a depth of 6 km, and thickness of 3 km, we can make the following estimates: Assuming a regional pre-intrusive temperature gradient of 50 °C km^{-1} (Figure 25) and a magma temperature of 800°C, the excess temperature at the top of the prism is 500°C. After 100,000 years the central temperature of the magma chamber will be only 100°C above ambient, and after 250,000 years, only 25°C above ambient. The average heat flow will increase from 100 to over 250 mW m^{-2}, but owing to the time lag and edge effects of the finite magma chamber, the maximum anomaly in the upper kilometer or so will not be seen for about 100,000 years, and will only amount to 10% of the initial average. Within the time frame of 100,000 to 250,000 years suggested by the geochronology, the anomaly between 2.5 and 3 km depth is fairly flat but amounts to only a 30 to 40°C increase over the 100 to 120°C estimates of Figure 25.

This model, with a volume of ~ 100 km^3, is conservative, but reasonable locally considering the observed surface volume of ~7 km^3. It is, however, dwarfed by the equally arbitrary estimate of 1,250 km^3 of Smith et al. (1978) for a magma chamber centered on San Francisco Mountain. Adoption of this estimate would result in estimated temperatures in the range of 200°C at drillable depths above the center of the magma chamber, but our study area would be near the eastern edge of the larger chamber, resulting in somewhat lower temperatures.

The foregoing calculations have very large uncertainties because of our lack of knowledge of the subsurface. They should be viewed simply as indicators of the sensitivity of the parameters to the age and dimensions of the magmatic heat source. To the extent that

we have assumed conductive cooling, they also represent an upper limit to the expected reservoir temperatures. Hydrothermal convection, for which there is hydrologic evidence, would hasten the cooling of the magma chamber and result in lower reservoir temperatures. On the other hand, as pointed out by Smith et al. (1978), silicic magma chambers have "a long prehistory of magmatic activity that represents additional thermal energy in the surrounding crustal rocks." Smith and Shaw (1975) also point out that, with respect to the "single shot" intrusion model, "Because many silicic volcanic systems are not closed, but continue to receive subchamber heating, this procedure gives minimum cooling time and heat contents for most systems." If there were younger episodes of mid-to-upper crustal intrusion that had no surface manifestations, we would also be underestimating possible reservoir temperatures. The Sunset Crater event gives us reason to believe that this is the case.

3. RECOMMENDATIONS FOR FURTHER STUDIES

We have summarized prior knowledge concerning the study area, and performed all of the surface-based studies that could constrain models for the deep thermal state of the easternmost part of the San Francisco Volcanic Field with the available resources. As stated above, even though the range of possible thermal conditions is large and uncertain, there is ample evidence from the ages of silicic volcanic rocks, the very young basaltic event at Sunset Crater to the south of our study area, and the evidence for mixing of magmatic fluids with the groundwater, that a contemporary hydrothermal system exists. The unique nature of the hydrology of the area, in particular the deep water table and the large lateral hydraulic gradients, yield the result that the depth, size, and temperature of this system remain indeterminate from surface studies

Only two credible options remain to be considered:

1. Archive our report, and because of the uncertainties, costs and risks involved in further exploration, abandon the Robinson Crater area as a possible geothermal resource for the foreseeable future. Further surface-based work would not add significantly to what we know presently.

2. Drill an exploratory well to resolve the ambiguities and uncertainties implicit in our report. The most cost-effective well would be a core hole, which would have the added advantage of characterizing the geologic section approximately midway between the two sites where most of it is exposed in outcrop (Grand Canyon and the Verde Valley). The site (Plate 2) is on private land-a patented mining claim. The property owners have been very interested in our work to date, and are willing to grant access for the drilling operation, subject to reasonable assurances regarding liability. Cost of the drilling operation by itself is estimated to be about $1 M, with a like amount for logging, testing, engineering, and compliance with environmental requirements.

We naturally favor option 2, and subject to finding partners who are willing to invest matching funds, we intend to submit a Phase II proposal to the GRED Program. We have some experience in exploratory drilling, but we do not possess the resources to do all the permitting, engineering design, flow tests and down-hole measurements required to assess the hydrothermal system if one is discovered. We intend to recruit the necessary expertise to fill out the Phase II team.

An important subsidiary benefit of proceeding with an exploratory core hole will be the opportunity for advances in scientific knowledge. As suggested in the second option, a continuous core will be extremely valuable in the interpretation of the geology of this part of the Colorado Plateau. Calibration of seismic parameters, characterizing the thermal/hydrologic regime of the study area, and constraining interpretation of other geophysical data will all be important products of the Phase II investigations.

4. PHASE II

We do not believe that further surface studies of the eastern San Francisco Volcanic Field will significantly increase the understanding of the possible geothermal system at depth. The only tool to explore this system further is the drill. This project should therefore move into the Department of Energy, Project GRED II Classification Phase II, Drilling and Characterization. A rough estimate to how this next phase of the project is expected to look is outlined below:

a) Cost estimate

Drilling to 8-10,000 feet, including coring the Precambrian section:	$1,200,000
Well-logging, flow testing, core analysis and other technical/science support:	500,000
Total	$1,700,000

b) Project Duration:

2 years

c) Project Management:

Lead Agency: Northern Arizona University, working in partnership with Industrial Sponsor(s)

Other Major Organizations:

Geothermal Engineering Consultant - Permitting, Land, Road/Access Negotiation, Day-to-Day Drilling Supervision, etc.

Drilling Company

Well Logging/Flow testing Company(ies)

c) Funding Sources:

Department of Energy, Project GRED II:	$800,000
Private Industry/Other Sources:	$900,000

d) Drilling Site:

The proposed drilling site is on a parcel of land that is a patented mining claim on the north side of Robinson Crater, approximately 1¼ miles west southwest on O'Leary Peak (see site indicated on Plate 2). This land is currently in use as a hard rock quarry for rhyolite, and informal negotiations with the owners indicate that they will be glad to cooperate with the project and allow drilling on their land.

e) Drilling Permitting and Permissions:

The proposed drilling site is enclosed by The Coconino National Forest, so permitting and permissions will be required from the Forest Service to access the site. However, as the site is on land that is an active quarry with several large trucks hauling crushed rock out of the site per day, and heavy equipment already operating on the site, we do not anticipate problems with this process. An environmental impact statement may be

required, especially for flow tests, by the size of the parcel of land is adequate to contain any drilling mud or fluids produced within the site for later removal. One of the tasks of the Geothermal Consulting Engineer will be to oversee the permitting process and to ensure that all legal requirements of the project are met, including environmental concerns.

f) Estimated Timetable:

As soon as possible – The project could start as early as Fall/Winter 2004, depending on funding.

ACKNOWLEDGEMENTS

This study was funded through Agreement # DE-FC04-2002AL68298 of the GRED II program of the U. S. Department of Energy, with generous matching funds arranged by Mr. Timothy McDonald, from APS, a Pinnacle West Company, and with matching funds from Northern Arizona University. Precision geographical positioning system equipment, and associated computing equipment, purchased for this project with funds from APS have been donated to the Department of Geology at Northern Arizona University at the completion of the project for continued use in the education and training of geology students and students other earth science related courses.

REFERENCES CITED

Bills, D. J., and Flynn, M. E., 2002, Hydrogeologic data for the Coconino Plateau and adjacent areas, Coconino and Yavapai counties, Arizona, *U.S. Geological Survey Open-File Report 02-0265*, 13 pp.

Bills, D. J., Truini, M., Flynn, M. E., Pierce, H. A., Catchings, R. D., and Rymer, J., 2000, Hydrogeology of the regional aquifer near Flagstaff, Arizona, 1994-97, *U.S. Geological Survey Open-File Report 00-4122*, 143 pp., 4 sheets.

Chronic, Halka, 2003, *Roadside Geology of Arizona*, Mountain Press Publishing, Missoula, Montana, 322 pp.

Crossey, L. J., Fischer, T. P., Patchett, P. J., Karlsrtom, K. E., Hilton, D. R., Huntoon, P., and Reynolds, A. C., 2004, Dissected hydrologic system at Grand Canyon: interaction between upper world and lower world waters in modern springs and travertine, submitted to *Bull., Geol. Soc. Am*., Jan. 2004, 14 pp., 3 tables and 8 figures.

Dalrymple, G.B., and Hirooka, K., 1965, Variation of potassium, argon, and calculated age in a Late Cenozoic basalt, *J. Geophys. Res., 70,* 5291-5296.

Damon, P.E., Laughlin, A.W., and Percious, J.K., 1967, Problems of excess argon-40 in volcanic rocks: in *Radioactive Dating and Methods of Low-Level Counting*, International Atomic Energy, Vienna, pp. 463-481.

Damon, P.R., Shafiqullah, M., and Leventhal, J.S., 1974, K-Ar Chronology for the San Francisco volcanic field and rate of erosion of the Little Colorado River: *Geological Society of America Rocky Mountain Section Meeting Field Trips, Geology of Northern Arizona, Part I – Regional Studies*, pp. 221-235.

Duffield, W. A., 1997, *Volcanoes of Northern Arizona*, Grand Canyon Association, Grand Canyon, Arizona, 68 pp.

Duffield, W. A., Morgan, P, and Sass, J. H., 2000, Untapped potential? The San Francisco volcanic field, Arizona, *Geothermal Resources Council, Bulletin, 29(3)*, 97-99.

Durrani, B. A., Doser, D. I., Keller, G. R., and Hearn, T. M., 1999, Velocity structure of the upper crust under the San Francisco volcanic field, Arizona, *Bull., Seism. Soc. Am., 89*, 239-249.

Hildreth, E.W., 1981, Gradients in Silicic Magma Chambers: Implications for Lithospheric Magmatism: *J. Geophys. Res., 86*, 10153-10192.

Holm, R F., 1988, Geologic Map of San Francisco Mountain, Elden Mountain, and Dry Lake Hills, Coconino County, Arizona: *U.S. Geological Survey Map I-1663*, 1:24,000.

Lachenbruch, A. H., and Sass, J. H., 1977, Heat flow in the United States and the thermal regime of the crust, in Heacock, J G; Keller, G V; Oliver, J E; Simmons, G, eds. *The Earth's Crust; its Nature and Physical Properties*, Geophysical Monograph, no.20, Am Geophys. Un., Washington, D.C., pp.626-675,

Lachenbruch, A. H., Sass, J. H., Munroe, R. J., and Moses, T. H., Jr., 1976, Geothermal setting and simple heat conduction models for the Long Valley Caldera, *J. Geophys. Res., .81*,.769-784.

Laney, P., and Brizzee, J., 2003, *Arizona Geothermal Resources*, *Idaho National Engineering and Environmental Laboratory Pubn, No. INEEL/MIS-2002-1616*, U. S. Dept. Energy, Office of Energy Efficiency and Renewable Energy geothermal Technologies Program, Map 1:500,000.

Luedke, R.G., and Smith, R.L., 1978, Map Showing Distribution, Composition, and Age of Late Cenozoic Volcanic Centers in Arizona and New Mexico: *U.S. Geological Survey Map I-1091-A*, 1:1,000,000.

Malotki, E., and Lomatuway'ma, M., 1987, *Earth Fire: A Hopi Legend of the Sunset Crater Eruption*: Northland Press, Flagstaff, Arizona.

Mickus, K. L., and Durrani, B., 1996, Gravity and magnetic study of the crustal structure of the San Francisco volcanic field, Arizona, USA, *Tectonophysics, 267*, 73-90.

Moore, R. B., and Wolfe, E. W., Geologic Map of the East Part of the San Francisco Volcanic Field, North-Central Arizona, *U. S. Geological Survey Map MF-1960*, 1:50,000.

Ort, M.H., Elson, M.D., and Champion, D.E., 2002, A Paleomagnetic Dating Study of Sunset Crater Volcano: *Technical Report No. 2002-16*, Desert Archaeology, Inc., Tucson, Arizona

Peters, L., 2003, $^{40}Ar/^{39}Ar$ Geochronology Results: *New Mexico Geochronological Research Laboratory Internal Report # NMGRL-IR-360*: attached as Appendix A.

Sass, J. H., Lachenbruch, A. H. Munroe, R.J. Greene, G. W., and Moses, T. H., Jr., 1971, Heat flow in the western United States, *J. Geophy. Res., 76*, 6376-6413.

Sass, J. H., Stone, C., and Bills, D. J.,1982, Shallow subsurface temperatures and some estimates of heat flow from the Colorado Plateau of northeastern Arizona, *U. S. Geological Survey, Open-File Report OF 82-0994*, 112 pp.

Sass, J. H., Lachenbruch, A.H., Galanis, S. P., Jr; Morgan, P., Priest, S. S., Moses, T. H., Jr. and Munroe, R. J., 1994, Thermal regime of the southern Basin and Range Province; 1, Heat flow data from Arizona and the Mojave Desert of California and Nevada, *J. Geophys. Res., 99*, 22,093-22,119.

Self, S., 1990, Sunset Crater, Arizona: in *Volcanoes of North America*, Cambridge University Press, pp. 280-281.

Shoemaker, E. M., Squires, R. L., and Abrams, M. J., 1978, Bright Angel and Mesa Butte fault systems of northern Arizona, in R. B. Smith and G. P. Eaton, eds., *Cenozoic Tectonics and Regional Geophysics of the Western Cordillera*, Geological Society of America Memoir 152, 341-367.

Smiley, T.C., 1958, The Geology and Dating of Sunset Crater, Flagstaff, Arizona: in *New Mexico Geologic Society, 9th Field Conference Guidebook of the Black Mesa Basin*, p. 186-190.

Smith, R. L., and Shaw, H. R., 1975, Igneous-related geothermal systems, in Assessment of Geothermal Resources of the United States, *U. S. Geological Survey Circular C 0726*, pp.58-83.

Smith, R.L., and Shaw, H.R., 1979, Igneous-Related Geothermal Systems: *U.S. Geological Survey Circular 790*, pp. 12-17.

Smith, R.L., Shaw, H.R., Luedke, R.G., and Russell, S.L., 1978, Comprehensive Tables Giving Physical Data and Thermal Energy Estimates for Young Igneous Systems of the United States: *U.S. Geological Survey Open-File Report 78-925*, 15 pp.

Stauber, D. A., 1982., Two-dimensional compressional wave velocity structure under San Francisco volcanic field, Arizona, from teleseismic *P* residual measurements, *J. Geophys. Res., 87*, 5451-5459.

Swanberg, C. A., and Morgan, P., 1979, The linear relation between temperatures based on the silica concentration of groundwater and regional heat flow: a new heat flow map of the United States, *Pure Appl. Geophys., 117*, 227-241.

Swanberg, C. A., and Morgan, P., 1985, Silica heat flow estimates and heat flow in the Colorado Plateau and adjacent areas, *J. Geodynamics, 3*, 65-85.

Tanaka, K.L., Shoemaker, E.M., Ulrich, G.E., and Wolfe, E.W., 1986, Migration of Volcanism in the San Francisco Volcanic Field, Arizona: *Bull., Geol. Soc. Am., 97*, 129-141.

Taylor, J. A., 1997, *Hydrothermal Regimes of the San Francisco Volcanic Field and the Southern Verde Valley, North-Central, Arizona*, M. S. Thesis, Northern Arizona University, May 1997, 95 pp.

Towle, J. N., 1984, The anomalous geomagnetic variation field and geoelectric structure associated with the Mesa Butte fault system, Arizona, *Bull., Geol. Soc. Am., 95,* 221-225.

Ulrich, G.E., Billingsley, G.H., Hereford, R., Wolfe, E.W., Nealey, L.D., and Sutton, R.L., 1984, Map Showing Geology, Structure, and Uranium Deposits of the Flagstaff 1 x 2 degree Quadrangle, Arizona: *U.S. Geological Survey Map I-1446*, 1:250,000.

Wilson, M., 1989, *Igneous Petrogenesis*, HarperCollins, London, 466 pp.

Wolfe, E.W., 1990, San Francisco, Arizona, in *Volcanoes of North America*, Cambridge University Press, p. 278-280.

Wolfe, E.W., Ulrich, G.E., Moore, R.B., Newhall. C.G., Holm, R.F., and Bailey, N.G., 1987, *U.S. Geological Survey Maps I-1956, I-1957, I-1958, I-1959, I-1960*, 1:50,000.

Appendix A: Geochronology data and plots from the New Mexico Geochronology Research Laboratory

$^{40}Ar/^{39}Ar$ Geochronology Results

By

Lisa Peters

DECEMBER 3, 2003

Prepared for

Wendell Duffield
Geology Department
Northern Arizona University
Flagstaff, AZ 86011

NEW MEXICO
GEOCHRONOLOGICAL RESEARCH LABORATORY
(NMGRL)

CO-DIRECTORS	LABORATORY TECHNICIANS
DR. MATTHEW T. HEIZLER	LISA PETERS
DR. WILLIAM C. MCINTOSH	RICHARD P. ESSER

Internal Report # : NMGRL-IR-**360**

Introduction

This report presents $^{40}Ar/^{39}Ar$ dating results from a set of seven volcanic samples from Arizona, submitted for dating by Wendell Duffield.

$^{40}Ar/^{39}Ar$ Analytical Methods and Results

Sanidine was separated from samples DL-2, SL-1 and O'Leary Peak. These samples were crushed and cleaned with dilute hydrofluoric acid and distilled water. The sanidine was separated with standard heavy liquid, magnetic separator and handpicking techniques. No sanidine was found in samples Strawberry Crater, Deadman Mesa, RC1 or SLN-1. Groundmass concentrates were prepared from Strawberry Crater and Deadman Mesa by crushing, cleaning with dilute hydrochloric acid and handpicking techniques. The mineral separates were loaded into aluminum discs and irradiated for 1 hour at the Nuclear Science Center in College Station, Texas.

Sanidine from O'Leary Peak, DL-2 and SL-1 were step-heated as bulk separates with the CO_2 laser, whereas groundmass from Deadman Mesa and Strawberry Crater were analyzed by the furnace incremental heating age spectrum method. Abbreviated analytical methods for these samples are given in Table 1, and details of the overall operation of the New Mexico Geochronology Research Laboratory are provided in the Appendix. The argon isotopic results are summarized in Table 1 and listed in Tables 2 and 3.

Sanidine from O'Leary Peak yielded a somewhat disturbed age spectrum (Figure A1a). Step H reveals the youngest apparent age (0.271±0.006 Ma) calculated from the age spectrum analysis. Inverse isochron analysis of steps A-J reveals a $^{40}Ar/^{36}Ar$ intercept that agrees within error (295.2±5.6) to the atmospheric ratio of 295.5 (Figure A1b).

Sanidine from SL-1 yields a saddle-shaped age spectrum (Figure A2a). Radiogenic yields and K/Ca values roughly rise as the apparent ages fall. Step F reveals the youngest apparent age (0.091±0.001 Ma) calculated from the age spectrum analysis. Inverse isochron analysis of steps A –G reveals a $^{40}Ar/^{36}Ar$intercept (301.8±7.8) within error of the atmospheric intercept and an isochron age of 0.093±0.016Ma(Figure A2b).

DL-2 sanidine yields a highly disturbed age spectrum with anomalously old apparent ages (as old as 16.85 Ma) in the early and late heating steps (Figure A3a). A weighted mean age of 1.73±0.02 Ma is calculated from steps C-D. The data was evaluated with the inverse isochron technique and found to be nonisochronous (Figure A3b).

Groundmass concentrates from Deadman Mesa and Strawberry Crater yield slightly disturbed age spectra (Figures A4a and A5a). Both reveal K/Ca values that decrease over the entire age spectrum and overall low (<20%) radiogenic yields. Weighted mean ages of 0.25±0.03 Ma for Deadman Mesa and 0.13±0.04 Ma for Strawberry Crater are calculated from 100% of the ^{39}Ar released. Inverse isochron analysis of steps A-I reveal s $^{40}Ar/^{36}Ar$ intercepts (296.0±4.1, Deadman Mesa and 292.9±4.6, Strawberry Crater) that agree within error to the atmospheric value (Figures A4b and A5b).

Discussion

There are multiple explanations for the disturbed age spectra revealed by the analyses of O'Leary, SL-1, and DL-2. Xenocrystic contaminants and excess Ar ($^{40}Ar/^{36}Ar > 295.5$, the atmospheric ratio) would have the affect of making the apparent ages older than the actual eruption age of the rocks. Alteration and accompanying Ar loss would result in apparent ages younger than the actual eruption ages. The inverse isochrons from DL-2, SL-1 and possibly to a lesser extent O'Leary are consistent with what we would expect to see if the separates contained a mix of ages (multiple $^{39}Ar/^{40}Ar$ intercepts) that are at least partially thermally distinct. This, combined with the atmospheric intercepts revealed by steps A-G of SL-1 and A-J of O'Leary make it seem likely that all three have some degree of xenocrystic contamination. The apparent ages assigned to these samples are the age of the youngest step or in the case of DL-2 a weighted mean of two adjoining steps that agree within error (O'Leary, 0.271±0.06 Ma; SL-2, 0.091±0.001 Ma; and DL-2, 1.73±0.02 Ma). These ages are assigned as maximum eruption ages. We do caution that if the sanidine has undergone Ar loss (during alteration), the assigned ages could be younger than the actual eruption age. The ages assigned as the eruption ages of Deadman Mesa and Strawberry Crater are the weighted mean ages calculated from the age spectra analyses (0.25±0.03 Ma and 0.13±0.04 Ma, respectively).

References Cited

Deino, A., and Potts, R., 1990. Single-Crystal $^{40}Ar/^{39}Ar$ dating of the Olorgesailie Formation, Southern Kenya Rift, J. Geophys. Res., 95, 8453-8470.

Deino, A., and Potts, R., 1992. Age-probability spectra from examination of single crystal $^{40}Ar/^{39}Ar$ dating results: Examples from Olorgesailie, Southern Kenya Rift, Quat. International, 13/14, 47-53.

Mahon, K.I., 1996. The New "York" regression: Application of an improved statistical method to geochemistry, International Geology Review, 38, 293-303.

Samson, S.D., and, Alexander, E.C., Jr., 1987. Calibration of the inter-laboratory $^{40}Ar/^{39}Ar$ dating standard, Mmhb-1, Chem. Geol., 66, 27-34.

Steiger, R.H., and Jäger, E., 1977. Subcommission on geochronology: Convention on the use of decay constants in geo- and cosmochronology. Earth and Planet. Sci. Lett., 36, 359-362.

Taylor, J.R., 1982. An Introduction to Error Analysis: The Study of Uncertainties in Physical Measurements,. Univ. Sci. Books, Mill Valley, Calif., 270 p.

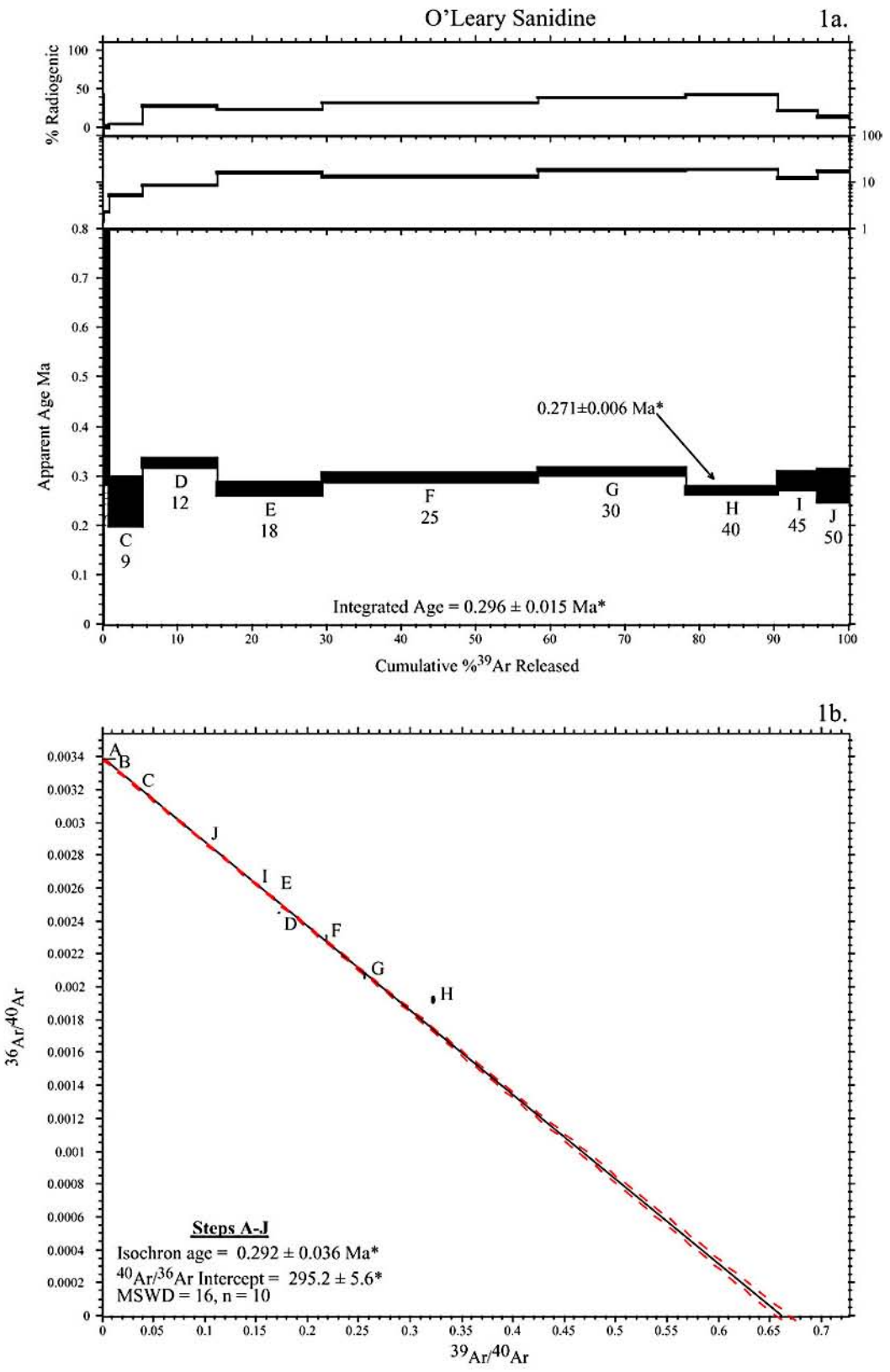

Figure A1. Age spectrum (a) and isochron (b) for sample O'Leary sanidine. *2sigma

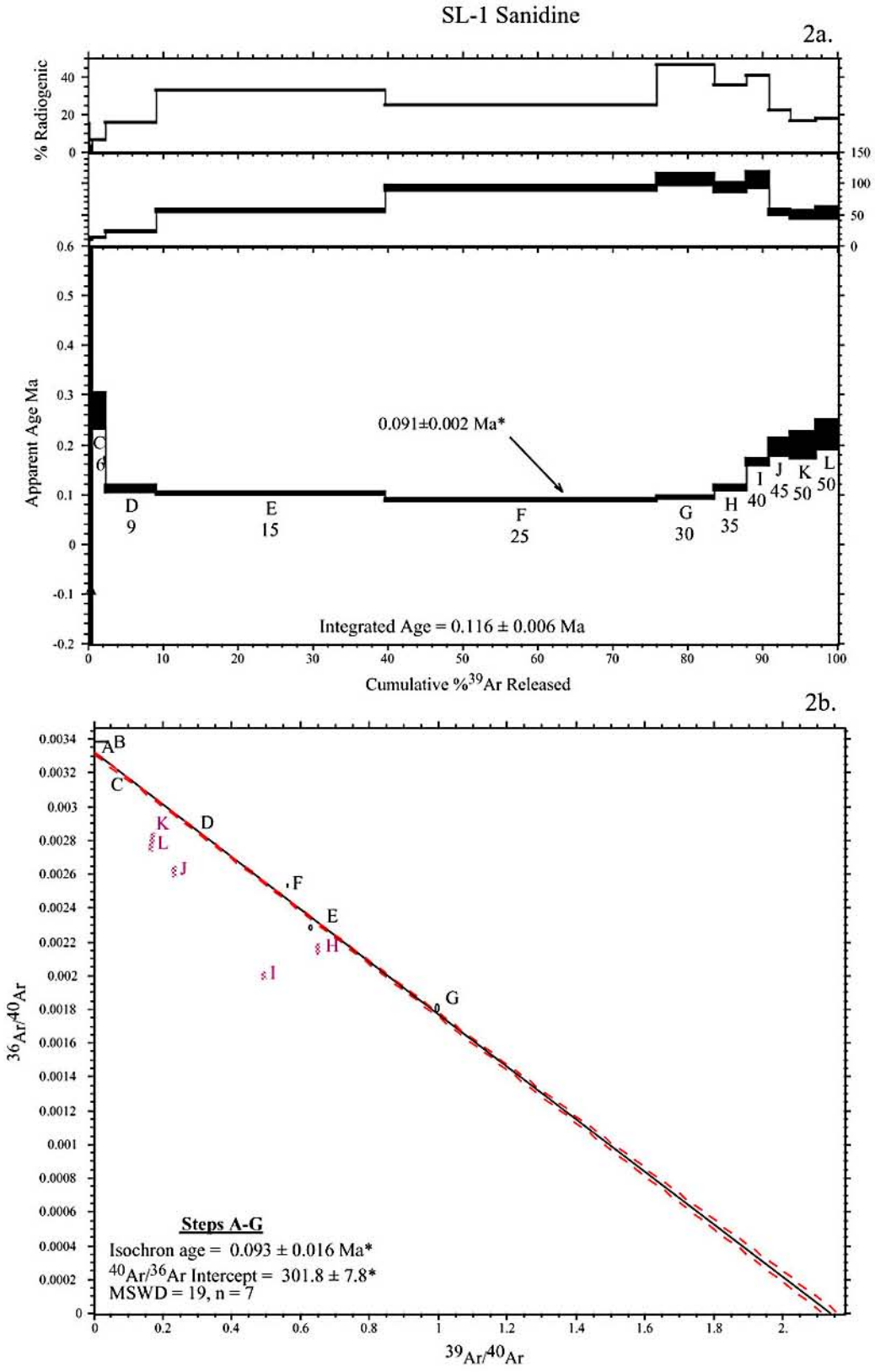

Figure 2. Age spectrum (a) and isochron (b) for sample SL-1 sanidine. Points shown in purple not included in isochron. *2sigma

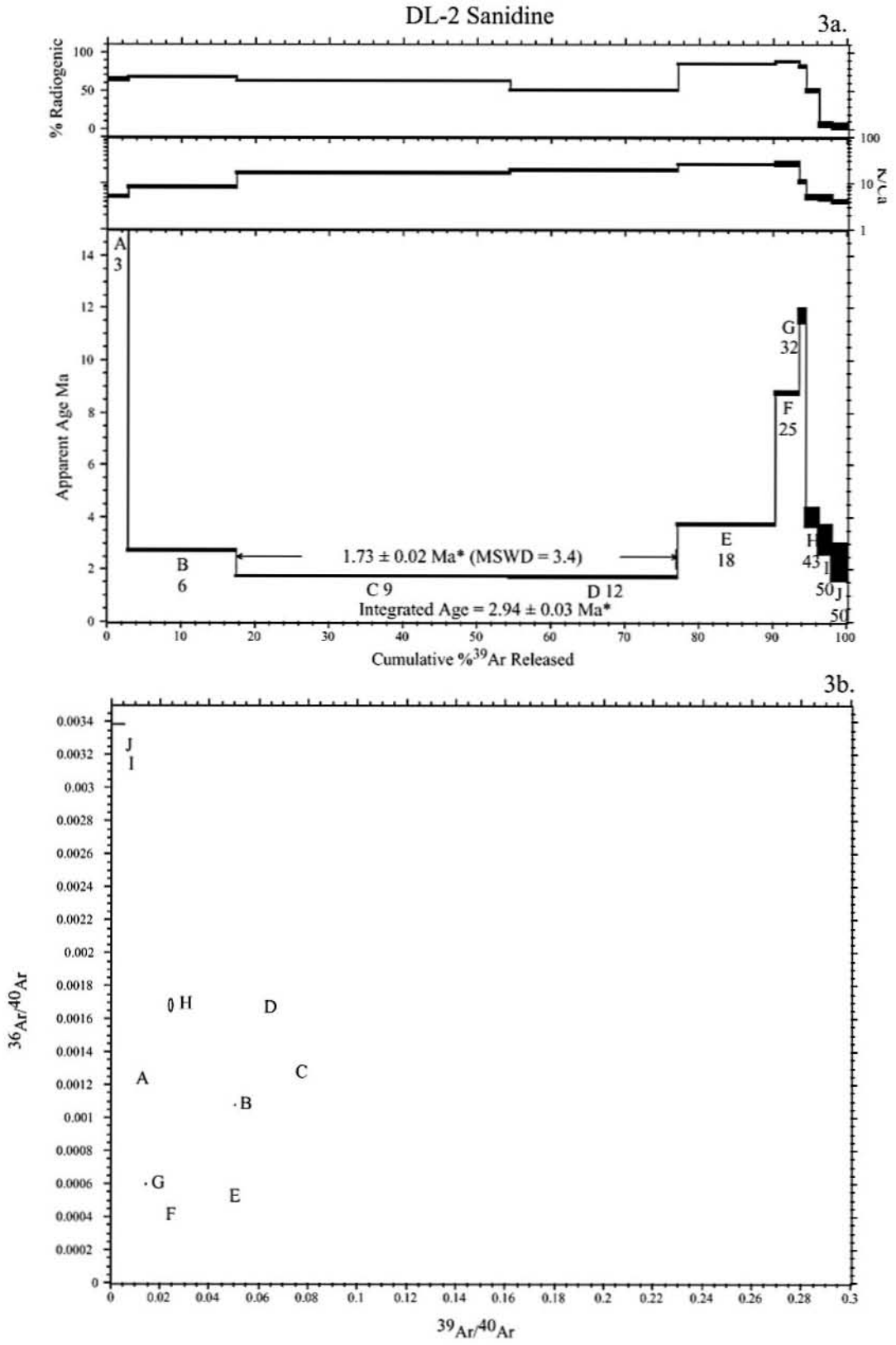

Figure A3. Age spectrum (a) and isochron (b) for sample DL-1 sanidine. *2sigma

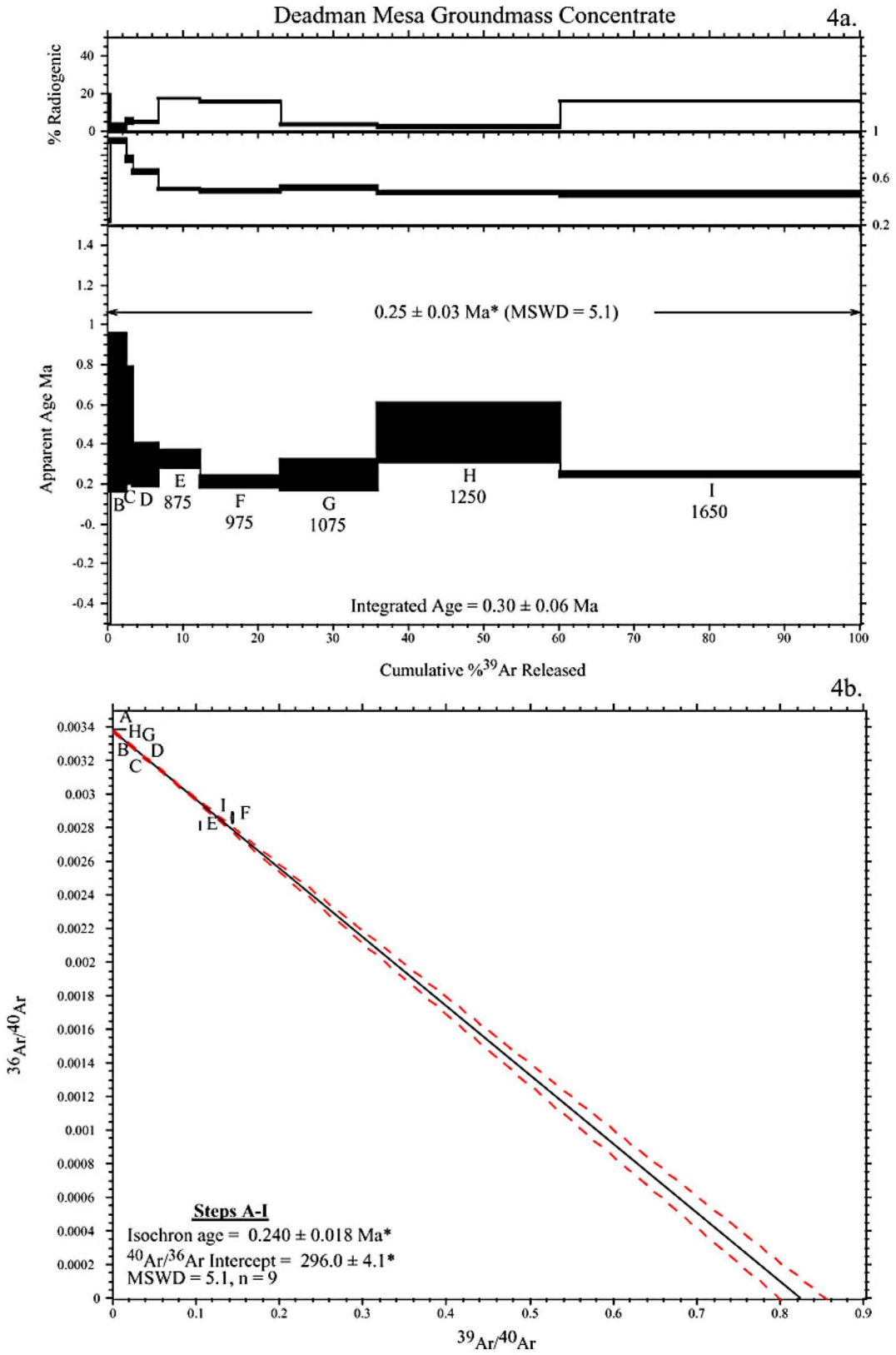

Figure A4. Age spectrum (a) and isochron (b) for sample Deadman Mesa groundmass concentrate. *2sigma

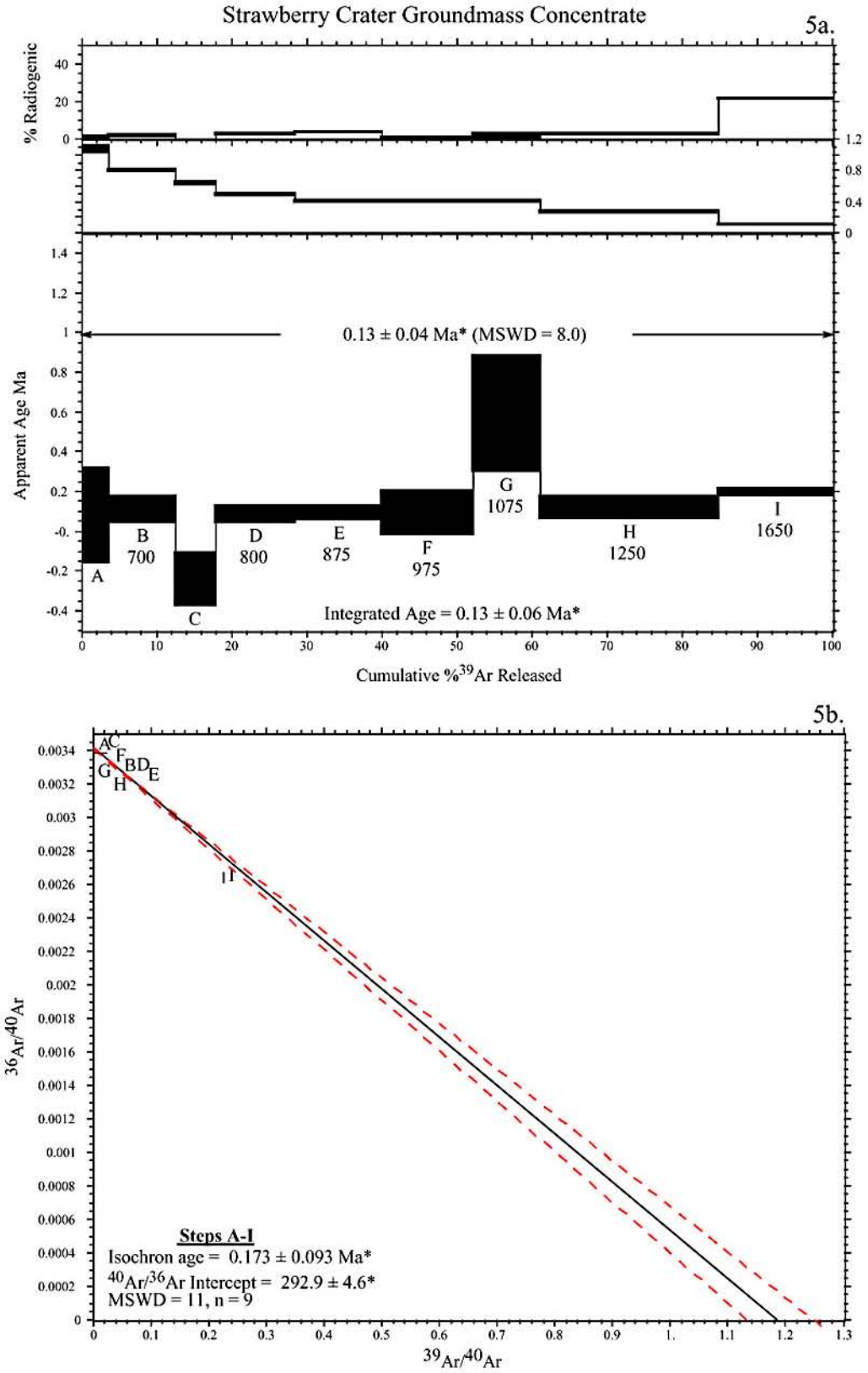

Figure A5. Age spectrum (a) and isochron (b) for sample Strawberry Crater. *2sigma

Table A1. Summary of $^{40}Ar/^{39}Ar$ results and analytical methods

Sample	Lab #	Irradiation	mineral	Age analysis	# of steps	Age	±2~	comments
Oleary Peak	53962	NM-163	sanidine	laser step-heat	1	0.271	0.006	Maximum eruption age
SL-1	53964	NM-163	sanidine	laser step-heat	1	0.091	0.002	Maximum eruption age
DL-2	53963	NM-163	sanidine	laser step-heat	2	1.73	0.02	Maximum eruption age
Deadman Mesa	54240	NM-169	groundmass concentrate	furnace step-heat	9	0.25	0.03	Slightly disturbed age spectrum
Strawberrry Crater	54241	NM-169	groundmass concentrate	furnace step-heat	9	0.13	0.04	Slightly disturbed age spectrum

Sample preparation and irradiation:
Mineral separates were prepared using standard crushing, dilute acid treatment, heavy liquid and hand-picking techniques.
Separates were loaded into a machined Al disc and irradiated for 1 hour in the D-3 position, Nuclear Science Center, College Station, TX. Neutron flux monitor Fish Canyon Tuff sanidine (FC-1). Assigned age = 27.84 Ma (Deino and Potts, 1990) relative to Mmhb-1 at 520.4 Ma (Samson and Alexander, 1987).

Instrumentation:
Mass Analyzer Products 215-50 mass spectrometer on line with automated all-metal extraction system.
Sanidine separates were step-heated with a 50 watt Synrad CO_2 laser.
Reactive gases removed during a 5.3 minute reaction with 2 SAES GP-50 getters, 1 operated at ~450°C and 1 at 20°C. Gas also exposed to a W filament operated at ~2000°C and a cold finger operated at -140°C.
Groundmass concentrates were step-heated using a Mo double-vacuum resistance furnace. Heating duration in the furnace was 10 minutes. Reactive gases removed during furnace analysis by reaction with 3 SAES GP-50 getters, 2 operated at ~450°C and 1 at 20°C. Gas also exposed to a W filament operated at ~2000°C.

Analytical parameters:
Electron multiplier sensitivity averaged 1.55 x 10-16 moles/pA for laser NM-163 samples and 2.64 x 10-16 moles/pA for NM-169 furnace samples.
Total system blank and background averaged 18000, 7.4, 1.3, 2.9, 6.3x 10^{-18} moles at masses 40, 39, 38, 37 and 36, respectively for the laser analyses, and 1890, 19.3, 0.33, 9.4, 5.5 x 10^{-18} moles at masses 40, 39, 38, 37 and 36, respectively for the furnace analyses. J-factors determined to a precision of ± 0.1% by CO_2 laser-fusion of 4 single crystals from each of 4 or 6 radial positions around the irradiation tray. Correction factors for interfering nuclear reactions were determined using K-glass and CaF_2 and are as follows:
$(^{40}Ar/^{39}Ar)K = 0.00020\pm0.0003$; $(^{36}Ar/^{37}Ar)_{Ca} = 0.00028\pm0.000005$; and $(^{39}Ar/^{37}Ar)_{Ca} = 0.0007\pm0.00002$.

Table A2. $^{40}Ar/^{39}Ar$ analytical data.

ID	Power (Watts)			$^{40}Ar/^{39}Ar$	$^{37}Ar/^{39}Ar$	$^{36}Ar/^{39}Ar$ (x 10^{-3})	^{39}ArK (x 10^{-15} mol)	K/Ca	$^{40}Ar^*$ (%)	^{39}Ar (%)	Age (Ma)	±1~ (Ma)
	DL-2, D5:163, 83.62 mg sanidine, J=0.000112, D=1.00484, NM-163, Lab#=53963-01											
†	A	3	131.4	0.0993		161.0	3.28	5.1	63.8	2.7	16.85	0.17
†	B	6	19.86	0.0609		21.48	18.0	8.4	68.1	17.5	2.73	0.01
	C	9	13.76	0.0296		17.49	44.8	17.2	62.5	54.4	1.74	0.01
	D	12	16.67	0.0266		27.69	27.5	19.2	50.9	77.1	1.71	0.01
†	E	18	21.89	0.0194		11.30	16.1	26.2	84.8	90.3	3.74	0.01
†	F	25	49.33	0.0190		19.80	3.84	26.9	88.1	93.5	8.76	0.03
†	G	32	70.69	0.0466		42.26	1.07	11.0	82.3	94.3	11.72	0.15
†	H	43	39.57	0.1014		66.88	2.32	5.0	50.1	96.2	4.00	0.18
†	I	50	216.8	0.1036		680.6	2.06	4.9	7.2	97.9	3.17	0.28
†	J	50	278.9	0.1212		905.6	2.50	4.2	4.1	100.0	2.29	0.35
	Integrated age ± 2~			n=10			121.5		K2O=4.98	%	2.94	0.03
	Plateau ± 2~ steps C-D			n=2		MSWD=3.42	72.4	18.0		59.6	1.73	0.02
	SL-1, D6:163, 124.01 mg sanidine, J=0.0001116, D=1.00484, NM-163, Lab#=53964-01											
	A	1	1091.8	0.1107		3647.5	0.222	4.6	1.3	0.1	2.8	1.4
	B	3	306.5	0.0440		1033.4	0.70	11.6	0.4	0.4	0.230	0.285
	C	6	20.15	0.0377		63.68	4.6	13.5	6.6	2.3	0.269	0.019
	D	9	3.510	0.0218		9.983	16.7	23.4	16.0	9.0	0.113	0.004
	E	15	1.525	0.0089		3.438	75.3	57.6	33.4	39.5	0.103	0.001
	F	25	1.789	0.0055		4.530	89.8	93.3	25.2	75.9	0.091	0.001
	G	30	1.005	0.0048		1.813	18.7	106.7	46.8	83.4	0.095	0.001
	H	35	1.546	0.0054		3.338	10.5	94.5	36.3	87.7	0.113	0.003
	I	40	2.030	0.0048		4.062	7.7	106.0	40.9	90.8	0.167	0.003
	J	45	4.294	0.0093		11.24	6.8	54.7	22.7	93.6	0.196	0.009
	K	50	5.913	0.0103		16.65	8.4	49.6	16.8	97.0	0.200	0.014
	L	50	6.048	0.0095		16.74	7.5	53.9	18.2	100.0	0.222	0.014
	Integrated age ± 2~			n=12			247.1		K2O=6.86	%	0.116	0.006
	O'Leary, D4:163, 176.63 mg sanidine, J=0.0001119, D=1.00484, NM-163, Lab#=53962-01											
	A		3	4655.7	0.3037	15738.2	0.174	1.7	0.1	0.1	1.0	4.3
	B		6	232.2	0.2214	774.5	1.95	2.3	1.4	0.8	0.672	0.195
	C		9	30.01	0.1011	97.47	11.8	5.0	4.1	5.3	0.247	0.025
	D		12	5.832	0.0603	14.29	26.1	8.5	27.7	15.2	0.326	0.004
	E		18	5.971	0.0322	15.63	36.9	15.8	22.7	29.3	0.274	0.006
	F		25	4.594	0.0398	10.57	75.9	12.8	32.1	58.3	0.297	0.005
	G		30	3.916	0.0282	8.078	51.8	18.1	39.1	78.0	0.309	0.004
	H		40	3.143	0.0275	6.107	32.3	18.6	42.7	90.4	0.271	0.003
	I		45	6.694	0.0416	17.81	14.1	12.3	21.4	95.8	0.289	0.010
	J		50	10.00	0.0305	29.17	11.1	16.7	13.9	100.0	0.280	0.017
	Integrated age ± 2~			n=10			262.1		K2O=5.09	%	0.296	0.015

Notes:

Isotopic ratios corrected for blank, radioactive decay, and mass discrimination, not corrected for interfering reactions. Ages calculated relative to FC-1 Fish Canyon Tuff sanidine inter-laboratory

standard at 27.84 Ma. Errors quoted for individual analyses include analytical error only, without interfering reaction or J uncertainties. Integrated age calculated by recombining isotopic measurements of all steps. Integrated age error calculated by recombining errors of isotopic measurements of all steps. Plateau age is inverse-variance-weighted mean of selected steps. Plateau age error is inverse-variance-weighted mean error (Taylor, 1982) times root MSWD where MSWD>1. Plateau and integrated ages incorporate uncertainties in interfering reaction corrections and J factors. Decay constants and isotopic abundances after Steiger and Jäger (1977).

† symbol preceding sample ID denotes analyses excluded from plateau age calculations.

Discrimination = 1.00484 ± 0.00092

Correction factors:
$(^{39}Ar/^{37}Ar)C_a$ = 0.00072 ± 2e-05
$(^{36}Ar/^{37}Ar)C_a$ = 0.00028 ± 5e-06
$(^{38}Ar/^{39}Ar)K$ = 0.01077
$(^{40}Ar/^{39}Ar)K$ = 0.0002 ± 0.0003

Table A3. $^{40}Ar/^{39}Ar$ analytical data.

ID	Power (Watts)	$^{40}Ar/^{39}Ar$	$^{37}Ar/^{39}Ar$	$^{36}Ar/^{39}Ar$ (x 10^{-3})	^{39}ArK (x 10^{-15} mol)	K/Ca	$^{40}Ar^*$ (%)	^{39}Ar (%)	Age (Ma)	±1~ (Ma)
Deadman Mesa, D3:165, 186.55 mg groundmass concentrate, J=0.0001096, D=1.00562, NM-169, Lab#=54240-01										
A	575	1669.1	0.8389	5750.8	0.236	0.61	-1.8	0.2	-6.0	2.1
B	650	136.1	0.2162	451.2	2.98	2.4	2.1	2.5	0.56	0.20
C	700	48.11	0.2599	154.4	1.04	2.0	5.2	3.3	0.49	0.15
D	750	29.41	0.7745	94.55	4.49	0.66	5.1	6.7	0.30	0.06
E	825	9.560	0.3881	26.94	7.07	1.3	17.1	12.2	0.32	0.02
F	925	6.883	0.4023	19.86	13.9	1.3	15.2	22.9	0.21	0.01
G	1025	35.80	0.3796	117.1	16.9	1.3	3.4	35.9	0.24	0.04
H	1200	101.9	0.4113	337.3	31.5	1.2	2.3	60.2	0.45	0.07
I	1600	7.952	0.4228	22.81	51.8	1.2	15.7	100.0	0.25	0.01
Integrated age ± 2~			n=9		129.9		K_2O=2.44 %		0.30	0.06
Plateau ± 2~ steps A-I			n=9	MSWD=5.11	129.9	1.3		100.0	0.25	0.03
Strawberry Crater, D4:165, 191.07 mg groundmass concentrate, J=0.0001138, D=1.00562, NM-169, Lab#=54241-01										0.12
A	575	114.3	0.1832	385.5	5.36	2.8	0.4	3.6	0.08	
B	650	22.76	0.2457	75.26	13.4	2.1	2.4	12.4	0.11	0.03
C	700	62.11	0.3062	214.2	8.0	1.7	-1.9	17.7	-0.24	0.07
D	750	14.65	0.3943	48.33	15.9	1.3	2.7	28.3	0.08	0.02
E	825	11.94	0.4824	39.08	17.5	1.1	3.7	39.9	0.09	0.02
F	925	63.03	0.4879	212.0	18.2	1.0	0.7	52.0	0.09	0.05
G	1025	174.9	0.4862	582.3	13.6	1.0	1.6	61.0	0.58	0.14
H	1200	20.73	0.7323	68.58	35.6	0.70	2.5	84.6	0.11	0.03
I	1600	4.452	1.762	12.99	23.2	0.29	17.0	100.0	0.16	0.01
Integrated age ± 2~			n=9		150.6		K_2O=2.66 %		0.13	0.06
Plateau ± 2~ steps A-I			n=9	MSWD=7.99	150.6	1.1		100.0	0.13	0.04

Notes:

Isotopic ratios corrected for blank, radioactive decay, and mass discrimination, not corrected for interfering reactions. Ages calculated relative to FC-1 Fish Canyon Tuff sanidine inter-laboratory standard at 27.84 Ma. Errors quoted for individual analyses include analytical error only, without interfering reaction or J uncertainties. Integrated age calculated by recombining isotopic measurements of all steps. Integrated age error calculated by recombining errors of isotopic measurements of all steps. Plateau age is inverse-variance-weighted mean of selected steps. Plateau age error is inverse-variance-weighted mean error (Taylor, 1982) times root MSWD where MSWD>1. Plateau and integrated ages incorporate uncertainties in interfering reaction corrections and J factors. Decay constants and isotopic abundances after Steiger and Jäger (1977).

Discrimination = 1.00562 ± 0.00081

Correction factors:

$(^{39}Ar/^{37}Ar)C_a$ = 0.00072 ± 2e-05
$(^{36}Ar/^{37}Ar)C_a$ = 0.00028 ± 5e-06
$(^{38}Ar/^{39}Ar)K$ = 0.01077
$(^{40}Ar/^{39}Ar)K$ = 0.0002 ± 0.0003

Appendix B: New Mexico Geochronology Research Laboratory Procedures

New Mexico Bureau of Mines and Mineral Resources

Procedures of the New Mexico Geochronology Research Laboratory for the

Period June 1998 – present

Matthew Heizler
William C. McIntosh
Richard Esser
Lisa Peters

$^{40}Ar/^{39}Ar$ and K-Ar dating

Often, large bulk samples (either minerals or whole rocks) are required for K-Ar dating and even small amounts of xenocrystic, authigenic, or other non-ideal behavior can lead to inaccuracy. The K-Ar technique is susceptible to sample inhomogeneity as separate aliquots are required for the potassium and argon determinations. The need to determine absolute quantities (i.e. moles of $^{40}Ar^*$ and ^{40}K) limits the precision of the K-Ar method to approximately 1% and also, the technique provides limited potential to evaluate underlying assumptions. In the $^{40}Ar/^{39}Ar$ variant of the K-Ar technique, a sample is irradiated with fast neutrons thereby converting ^{39K} to ^{39}Ar through a (n,p) reaction. Following irradiation, the sample is either fused or incrementally heated and the gas analyzed in the same manner as in the conventional K-Ar procedure, with one exception, no argon spike need be added.

Some of the advantages of the $^{40}Ar/^{39}Ar$ method over the conventional K-Ar technique are:

1. A single analysis is conducted on one aliquot of sample thereby reducing the sample size and eliminating sample inhomogeneity.
2. Analytical error incurred in determining absolute abundances is reduced by measuring only isotopic ratios. This also eliminates the need to know the exact weight of the sample.
3. The addition of an argon spike is not necessary.
4. The sample does not need to be completely fused, but rather can be incrementally heated. The $^{40}Ar/^{39}Ar$ ratio (age) can be measured for each fraction of argon released and this allows for the generation of an age spectrum.

The age of a sample as determined with the $^{40}Ar/^{39}Ar$ method requires comparison of the measured $^{40}Ar/^{39}Ar$ ratio with that of a standard of known age. Also, several isotopes of other elements (Ca, K, Cl, Ar) produce argon during the irradiation procedure and must be corrected for. Far more in-depth details of the determination of an apparent age via the $^{40}Ar/^{39}Ar$ method are given in Dalrymple et al. (1981) and McDougall and Harrison (1988).

Analytical techniques

Sample Preparation and irradiation details

Mineral separates are obtained in various fashions depending upon the mineral of interest, rock type and grain size. In almost all cases the sample is crushed in a jaw crusher and ground in a disc grinder and then sized. The size fraction used generally corresponds to the largest size possible which will permit obtaining a pure mineral separate. Following sizing, the sample is washed and dried. For plutonic and metamorphic rocks and lavas, crystals are separated using standard heavy liquid, Franz magnetic and hand-picking techniques. For volcanic sanidine and plagioclase, the sized sample is reacted with 15% HF acid to remove glass and/or matrix and then thoroughly washed prior to heavy liquid and magnetic separation. For groundmass concentrates, rock fragments are selected which do not contain any visible phenocrysts.

The NMGRL uses either the Ford reactor at the University of Michigan or the Nuclear Science Center reactor at Texas A&M University. At the Ford reactor, the L67

position is used (unless otherwise noted) and the D-3 position is always used at the Texas A&M reactor. All of the Michigan irradiations are carried out underwater without any shielding for thermal neutrons, whereas the Texas irradiations are in a dry location which is shielded with B and Cd. Depending upon the reactor used, the mineral separates are loaded into either holes drilled into Al discs or into 6 mm I.D. quartz tubes. Various Al discs are used. For Michigan, either six hole or twelve hole, 1 cm diameter discs are used and all holes are of equal size. Samples are placed in the 0, 120 and 240° locations and standards in the 60, 180 and 300° locations for the six hole disc. For the twelve hole disc, samples are located at 30, 60, 120, 150, 210, 240, 300, and 330° and standards at 0, 90, 180 and 270 degrees. If samples are loaded into the quartz tubes, they are wrapped in Cu foil with standards interleaved at ~0.5 cm intervals. For Texas, 2.4 cm diameter discs contain either sixteen or six sample holes with smaller holes used to hold the standards. For the six hole disc, sample locations are 30, 90, 150, 210, 270 and 330° and standards are at 0, 60, 120, 180, 240 and 300°. Samples are located at 18, 36, 54, 72, 108, 126, 144, 162, 198, 216, 234, 252, 288, 306, 324, 342 degrees and standards at 0, 90, 180 and 270 degrees in the sixteen hole disc. Following sample loading into the discs, the discs are stacked, screwed together and sealed *in vacuo* in either quartz (Michigan) or Pyrex (Texas) tubes.

Extraction Line and Mass Spectrometer details

The NMGRL argon extraction line has both a double vacuum Mo resistance furnace and a CO_2 laser to heat samples. The Mo furnace crucible is heated with a W heating element and the temperature is monitored with a W-Re thermocouple placed in a hole drilled into the bottom of the crucible. A one inch long Mo liner is placed in the bottom of the crucible to collect the melted samples. The furnace temperature is calibrated by either/or melting Cu foil or with an additional thermocouple inserted in the top of the furnace down to the liner. The CO_2 laser is a Synrad 10W laser equipped with a He-Ne pointing laser. The laser chamber is constructed from a 3 3/8" stainless steel conflat and the window material is ZnS. The extraction line is a two stage design. The first stage is equipped with a SAES GP-50 getter, whereas the second stage houses two SAES GP-50 getters and a tungsten filament. The first stage getter is operated at 450°C as is one of the second stage getters. The other second stage getter is operated at room temperature and the tungsten filament is operated at ~2000°C. Gases evolved from samples heated in the furnace are reacted with the first stage getter during heating. Following heating, the gas is expanded into the second stage for two minutes and then isolated from the first stage. During second stage cleaning, the first stage and furnace are pumped out. After gettering in the second stage, the gas is expanded into the mass spectrometer. Gases evolved from samples heated in the laser are expanded through a cold finger operated at -140°C and directly into the second stage. Following cleanup, the gas in the second stage and laser chamber is expanded into the mass spectrometer for analysis.

The NMGRL employs a MAP-215-50 mass spectrometer which is operated in static mode. The mass spectrometer is operated with a resolution ranging between 450 to 600 at mass 40 and isotopes are detected on a Johnston electron multiplier operated at ~2.1 kV with an overall gain of about 10,000 over the Faraday collector. Final isotopic intensities are determined by linear regression to time zero of the peak height versus time following gas introduction for each mass. Each mass intensity is corrected for mass spectrometer baseline and background and the extraction system blank.

Blanks for the furnace are generally determined at the beginning of a run while the furnace is cold and then between heating steps while the furnace is cooling. Typically, a blank is run every three to six heating steps. Periodic furnace hot blank analysis reveals that the cold blank is equivalent to the hot blank for temperatures less than about 1300°C. Laser system blanks are generally determined between every four analyses. Mass discrimination is measured using atmospheric argon which has been dried using a Ti-sublimation pump. Typically, 10 to 15 replicate air analyses are measured to determine a mean mass discrimination value. Air pipette analyses are generally conducted 2-3 times per month, but more often when samples sensitive to the mass discrimination value are analyzed. Correction factors for interfering nuclear reactions on K and Ca are determined using K-glass and CaF_2, respectively. Typically, 3-5 individual pieces of the salt or glass are fused with the CO_2 laser and the correction factors are calculated from the weighted mean of the individual determinations.

Data acquisition, presentation and age calculation

Samples are either step-heated or fused in a single increment (total fusion). Bulk samples are often step-heated and the data are generally displayed on an age spectrum or isochron diagram. Single crystals are often analyzed by the total fusion method and the results are typically displayed on probability distribution diagrams or isochron diagrams.

The Age Spectrum Diagram

Age spectra plot apparent age of each incrementally heated gas fraction versus the cumulative % $^{39}Ar_K$ released, with steps increasing in temperature from left to right. Each apparent age is calculated assuming that the trapped argon (argon not produced by *in situ* decay of ^{40}K) has the modern day atmospheric $^{40}Ar/^{36}Ar$ value of 295.5. Additional parameters for each heating step are often plotted versus the cumulative $\%^{39}Ar_K$ released. These auxiliary parameters can aid age spectra interpretation and may include radiogenic yield (percent of ^{40}Ar which is not atmospheric), K/Ca (determined from measured Ca-derived ^{37}Ar and K-derived ^{39}Ar) and/or K/Cl (determined from measured Cl-derived ^{38}Ar and K-derived ^{39}Ar). Incremental heating analysis is often effective at revealing complex argon systematics related to excess argon, alteration, contamination, ^{39}Ar recoil, argon loss, etc. Often low-temperature heating steps have low radiogenic yields and apparent ages with relatively high errors due mainly to loosely held, non-radiogenic argon residing on grain surfaces or along grain boundaries. An entirely or partially flat spectrum, in which apparent ages are the same within analytical error, may indicate that the sample is homogeneous with respect to K and Ar and has had a simple thermal and geological history. A drawback to the age spectrum technique is encountered when hydrous minerals such as micas and amphiboles are analyzed. These minerals are not stable in the ultra-high vacuum extraction system and thus step-heating can homogenize important details of the true ^{40}Ar distribution. In other words, a flat age spectrum may result even if a hydrous sample has a complex argon distribution.

The Isochron Diagram

Argon data can be plotted on isotope correlation diagrams to help assess the isotopic composition of Ar trapped at the time of argon closure, thereby testing the assumption that trapped argon isotopes have the composition of modern atmosphere which is implicit in age spectra. To construct an "inverse isochron" the $^{36}Ar/^{40}Ar$ ratio is plotted versus the $^{39}Ar/^{40}Ar$ ratio. A best fit line can be calculated for the data array which yields the value for the trapped argon (Y-axis intercept) and the $^{40}Ar^*/^{39}Ar_K$ value (age) from the X-axis intercept. Isochron analysis is most useful for step-heated or total fusion data which have a significant spread in radiogenic yield. For young or low K samples, the calculated apparent age can be very sensitive to the composition of the trapped argon and therefore isochron analysis should be preformed routinely on these samples (cf. Heizler and Harrison, 1988). For very old (>Mesozoic) samples or relatively old sanidines (>mid-Cenozoic) the data are often highly radiogenic and cluster near the X-axis thereby making isochron analysis of little value.

The Probability Distribution Diagram

The probability distribution diagram, which is sometimes referred to as an ideogram, is a plot of apparent age versus the summation of the normal distribution of each individual analysis (Deino and Potts, 1992). This diagram is most effective at displaying single crystal laser fusion data to assess the distribution of the population. The K/Ca, radiogenic yield, and the moles of ^{39}Ar for each analysis are also often displayed for each sample as this allows for visual ease in identifying apparent age correlations between, for instance, plagioclase contamination, signal size and/or radiogenic concentrations. The error (1s) for each age analysis is generally shown by the horizontal lines in the moles of ^{39}Ar section. Solid symbols represent the analyses used for the weighted mean age calculation and the generation of the solid line on the ideogram, whereas open symbols represent data omitted from the age calculation. If shown, a dashed line represents the probability distribution of all of the displayed data. The diagram is most effective for displaying the form of the age distribution (i.e. Gaussian, skewed, etc.) and for identifying xenocrystic or other grains which fall outside of the main population.

Error Calculations

For step-heated samples, a plateau for the age spectrum is defined by the steps indicated. The plateau age is calculated by weighting each step on the plateau by the inverse of the variance and the error is calculated by either the method of Samson and Alexander (1987) or Taylor (1982). A mean sum weighted deviates (MSWD) value is determined by dividing the Chi squared value by n-1 degrees of freedom for the plateau ages. If the MSWD value is outside the 95% confidence window (cf. Mahon, 1996; Table 1), the plateau or preferred age error is multiplied by the square root of the MSWD. For single crystal fusion data, a weighted mean is calculated using the inverse of the variance to weight each age determination (Taylor, 1982). Errors are calculated as described for the plateau ages above.

Isochron ages, $^{40}Ar/^{36}Ar_i$ values and MSWD values are calculated from the regression results obtained by the York (1969) method.

References Cited

Dalrymple, G.B., Alexander, E.C., Jr., Lanphere, M.A., and Kraker, G.P., 1981. Irradiation of samples for $^{40}Ar/^{39}Ar$ dating using the Geological Survey TRIGA reactor. U.S.G.S., Prof. Paper, 1176.

Deino, A., and Potts, R., 1990. Single-Crystal $^{40}Ar/^{39}Ar$ dating of the Olorgesailie Formation, Southern Kenya Rift, J. Geophys. Res., 95, 8453-8470.

Deino, A., and Potts, R., 1992. Age-probability spectra from examination of single-crystal $^{40}Ar/^{39}Ar$ dating results: Examples from Olorgesailie, Southern Kenya Rift, Quat. International, 13/14, 47-53.

Fleck, R.J., Sutter, J.F., and Elliot, D.H., 1977. Interpretation of discordant $^{40}Ar/^{39}Ar$ age-spectra of Mesozoic tholieiites from Antarctica, Geochim. Cosmochim. Acta, 41, 15-32.

Heizler, M. T., and Harrison, T. M., 1988. Multiple trapped argon components revealed by $^{40}Ar/^{39}Ar$ analysis, Geochim. Cosmochim. Acta, 52, 295-1303.

Mahon, K.I., 1996. The New "York" regression: Application of an improved statistical method to geochemistry, International Geology Review, 38, 293-303.

McDougall, I., and Harrison, T.M., 1988. Geochronology and thermochronology by the ^{40}Ar-^{39}Ar method. Oxford University Press.

Samson, S.D., and, Alexander, E.C., Jr., 1987. Calibration of the inter-laboratory $^{40}Ar/^{39}Ar$ dating standard, Mmhb-1, Chem. Geol., 66, 27-34.

Steiger, R.H., and Jäger, E., 1977. Subcommission on geochronology: Convention on the use of decay constants in geo- and cosmochronology. Earth and Planet. Sci. Lett., 36, 359-362. Taylor, J.R., 1982. An Introduction to Error Analysis: The Study of Uncertainties in Physical Measurements, Univ. Sci. Books, Mill Valley, Calif., 270 p.

York, D., 1969. Least squares fitting of a straight line with correlated errors, Earth and Planet. Sci. Lett.., 5, 320-324.